Allosteric Voltage Gating of Potassium Channels I
mSlo Ionic Currents in the Absence of Ca^{2+}

Frank T. Horrigan,* Jianmin Cui,‡ and Richard W. Aldrich*

From the *Department of Molecular and Cellular Physiology, Howard Hughes Medical Institute, Stanford University School of Medicine, Stanford, California 94305; and ‡Department of Biomedical Engineering, Case Western Reserve University, Cleveland, Ohio 44106

abstract Activation of large conductance Ca^{2+}-activated K^+ channels is controlled by both cytoplasmic Ca^{2+} and membrane potential. To study the mechanism of voltage-dependent gating, we examined mSlo Ca^{2+}-activated K^+ currents in excised macropatches from *Xenopus* oocytes in the virtual absence of Ca^{2+} (<1 nM). In response to a voltage step, I_K activates with an exponential time course, following a brief delay. The delay suggests that rapid transitions precede channel opening. The later exponential time course suggests that activation also involves a slower rate-limiting step. However, the time constant of I_K relaxation [$\tau(I_K)$] exhibits a complex voltage dependence that is inconsistent with models that contain a single rate limiting step. $\tau(I_K)$ increases weakly with voltage from −500 to −20 mV, with an equivalent charge (z) of only 0.14 e, and displays a stronger voltage dependence from +30 to +140 mV (z = 0.49 e), which then decreases from +180 to +240 mV (z = −0.29 e). Similarly, the steady state G_K–V relationship exhibits a maximum voltage dependence (z = 2 e) from 0 to +100 mV, and is weakly voltage dependent ($z \cong 0.4\ e$) at more negative voltages, where $P_o = 10^{-5}$–10^{-6}. These results can be understood in terms of a gating scheme where a central transition between a closed and an open conformation is allosterically regulated by the state of four independent and identical voltage sensors. In the absence of Ca^{2+}, this allosteric mechanism results in a gating scheme with five closed (C) and five open (O) states, where the majority of the channel's voltage dependence results from rapid C–C and O–O transitions, whereas the C–O transitions are rate limiting and weakly voltage dependent. These conclusions not only provide a framework for interpreting studies of large conductance Ca^{2+}-activated K^+ channel voltage gating, but also have important implications for understanding the mechanism of Ca^{2+} sensitivity.

key words: calcium • K_{Ca} channel • large conductance Ca^{2+}-activated K^+ channel • ion channel gating

introduction

Large conductance Ca^{2+}-activated K^+ (BK)[1] channels are sensitive to both membrane voltage and intracellular Ca^{2+} (Gorman and Thomas, 1980; Marty, 1981, Pallotta et al., 1981; Barrett et al., 1982; Latorre et al., 1982; Methfessel and Boheim, 1982; Moczydlowski and Latorre, 1983; DiChiara and Reinhart, 1995; Cui et al., 1997). The response of BK channels to Ca^{2+} is key to their physiological role in a variety of cell types and has been studied extensively (Lewis and Hudspeth, 1983; Magleby and Pallotta, 1983a,b; Petersen and Maruyama, 1984; Storm, 1987; Lancaster et al., 1991; McManus and Magleby, 1991; Brayden and Nelson, 1992; Bielefeldt and Jackson, 1993; Crest and Gola, 1993; Robitaille et al., 1993; Nelson et al., 1995; Yazejian et al., 1997; Marrion and Tavalin, 1998; Safronov and Vogel, 1998). Attempts to identify Ca^{2+}-binding sites have also provided a focus for structure–function studies (Wei et al., 1994; Schreiber and Salkoff, 1997; Schreiber et al., 1999). In comparison, the voltage-dependent activation of BK channels has received less attention. Yet BK channels respond rapidly to voltage changes (Hudspeth and Lewis, 1988; Cui et al., 1997), suggesting that this process might contribute to the physiological function of BK channels. More importantly, interactions between Ca^{2+}- and voltage-dependent activation (Cox et al., 1997a; Cui et al., 1997) imply that understanding BK channel Ca^{2+} sensitivity depends on also understanding the mechanism of voltage-dependent gating.

Voltage-dependent activation of BK channels occurs on a millisecond time scale, similar to many purely voltage-gated K^+ (K_v) channels. However, during an action potential, changes in voltage and voltage-dependent Ca^{2+} entry through Ca^{2+} channels contribute to BK channel activity such that the direct effect of voltage is difficult to assess. Using a spike-like voltage clamp, Crest and Gola (1993) examined the time course of Ca^{2+} and K currents during Ca^{2+} action potentials in molluscan neurons and concluded that BK channel voltage dependence is important for closing channels

Address correspondence to Dr. Richard W. Aldrich, Department of Molecular and Cellular Physiology, Howard Hughes Medical Institute, Stanford University School of Medicine, Stanford, CA 94305. Fax: 650-725-4463; E-mail: raldrich@leland.stanford.edu

[1]*Abbreviations used in this paper:* BK channels, large conductance Ca^{2+}-activated potassium channels; G–V, conductance–voltage relationship; MWC, Monod-Wyman-Changeux; WT, wild type.

rapidly following action potentials and for terminating repetitive firing in response to sustained depolarization. The properties of mammalian BK channel activation studied under constant $[Ca^{2+}]_i$ suggest they could participate in similar processes. The voltage sensitivity of BK channel activation is weak in comparison with that of K_v channels (Cui et al., 1997; Horrigan and Aldrich, 1999), but open probability (P_o) can increase from ~10 to 90% of P_{omax} in response to a 70-mV voltage change centered around the half-activation voltage (V_h) (Barrett et al., 1982; Cui et al., 1997). Calcium alters the kinetics of voltage-dependent activation and shifts V_h to more negative voltages (Barrett et al., 1982; Cui et al., 1997). Thus the change in P_o evoked by a given voltage stimulus can be "tuned" by $[Ca^{2+}]$.

Most studies of BK channel gating have been performed in the presence of Ca^{2+} (Barrett et al., 1982; Latorre et al., 1982; Moczydlowski and Latorre, 1983; McManus and Magleby, 1991; Rothberg and Magleby, 1998), leaving open the possibility that the mechanism of voltage sensitivity reflects, to some extent, voltage-dependent changes in the affinity of Ca^{2+} for its binding site rather than a direct effect of voltage on channel conformation (Moczydlowski and Latorre, 1983). Recent studies, however, involving several cloned homologues of the *slo* family of Ca^{2+}-activated K^+ channels demonstrate that BK channels can be activated by membrane depolarization in the absence of Ca^{2+} binding (Meera et al., 1996; Cui et al., 1997), and that gating currents can be detected under these conditions (Stefani et al., 1997; Horrigan and Aldrich, 1999). These and other results indicate that BK channel voltage sensitivity reflects the action of an intrinsic voltage sensor (Cui et al., 1997; Stefani et al., 1997). Indeed, the amino acid sequence of *slo* BK channels contains a "core" domain that has many features in common with that of K_v channels (Wei et al., 1994; Diaz et al., 1998). These include a p-region, homologous to the pore-forming region of K_v channels, surrounded by six putative transmembrane segments including a charged S4 domain. The S4 domain forms part of the voltage sensor of *Shaker* and other voltage-gated channels (Yang and Horn, 1995; Aggarwal and MacKinnon, 1996; Larsson et al., 1996; Mannuzzu et al., 1996; Seoh et al., 1996; Yang et al., 1996; Yusaf et al., 1996; Bao et al., 1999), and S4 mutations alter the voltage dependence of BK channels (Diaz et al., 1998; Cui, J., and R.W. Aldrich, manuscript in preparation). Thus, it is likely that structural and mechanistic similarities exist between BK and K_v channels.

In the present study, we examine the response of mSlo Ca^{2+}-activated K^+ channels to voltage in the virtual absence of Ca^{2+} (<1 nM, see methods) to help understand the mechanism of voltage-dependent gating. The behavior of mSlo in 0 Ca^{2+} must reflect transitions between only a subset of the states that are available in the presence of Ca^{2+}. Thus, the 0 Ca^{2+} condition should provide a limiting example of mSlo voltage-gating behavior that must be accounted for by any complete model of mSlo gating. The ability of BK channels to open in a voltage-dependent manner in the absence of Ca^{2+} suggests that channel activation is fundamentally a voltage-dependent process that is modulated by Ca^{2+} binding (Meera et al., 1996; Cox et al., 1997a). If so, the voltage-dependent activation pathway must be central to the Ca^{2+}-dependent response, and delineation of this pathway in the absence of Ca^{2+} will be a prerequisite to the establishment of a detailed Ca^{2+}-dependent gating scheme or the interpretation of BK channel structure–function studies that seek to distinguish Ca^{2+}- and voltage-dependent conformational changes.

Many of the effects of Ca^{2+} and voltage on the kinetic and steady state properties of macroscopic mSlo I_K can be reproduced by a gating scheme (Cox et al., 1997a) based on the allosteric model of Monod et al. (1965). According to this voltage-dependent Monod-Wyman-Changeux (MWC) scheme (Scheme I), mSlo channels activate by undergoing a rate limiting, voltage-dependent transition between a closed (C) and an open (O) conformation and Ca^{2+} binding alters the kinetic and equilibrium properties of this transition. Because mSlo channels are composed of four identical subunits (Shen et al., 1994), the model assumes that each channel contains four identical Ca^{2+} binding sites. This results in a scheme with 10 states representing different Ca^{2+}-bound versions of the closed and open conformation.

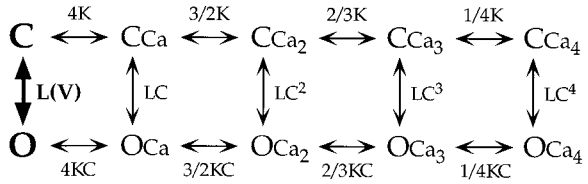

(SCHEME I)

A key feature of this model is that the C to O conformational change is allosteric in that it not only opens the channel pore, but also alters the Ca^{2+}-binding sites, causing their affinities for Ca^{2+} to increase. This allosteric linkage between channel opening and Ca^{2+} binding, represented by a factor, C, in the model, accounts for the ability of Ca^{2+} to affect open probability. Another important feature of the model is that the transition from C to O is represented by a single step and is therefore assumed to be concerted in the sense that Ca^{2+}-binding sites in all four subunits change simultaneously upon channel opening. Because the C–O transition is voltage

dependent, Scheme I also implicitly assumes that voltage sensors, presumably present in each subunit, move in a concerted manner during channel activation.

Although Scheme I reproduces many features of mSlo activation, it is likely to be an oversimplification, particularly with regards to the mechanism of voltage-dependent gating. A basic prediction of this model is that activation can be described by a simple two-state process in the absence of Ca^{2+} binding, indicated by the highlighted C–O transition in the above diagram. Although a two-state mechanism can account for the basic features of activation, deviations from Scheme I–like behavior are observed in the presence and absence of Ca^{2+} that suggest BK channel voltage gating is more complicated (Cox et al., 1997a). These deviations include a brief delay in voltage-dependent activation (Cox et al., 1997a; Stefani et al., 1997), and a conductance–voltage relationship (G–V) that is best fit by a Boltzmann function raised to a power greater than one (Cui et al., 1997). The shape of the G–V also changes slightly with $[Ca^{2+}]_i$, an effect that is not predicted by Scheme I (Cox et al., 1997a; Cui, J., and R.W. Aldrich, manuscript in preparation). Similarly, the voltage dependence of I_K relaxation kinetics deviates from the prediction of Scheme I at extreme voltages (Cox et al., 1997a). Finally, a rapid component of gating charge movement is observed that precedes channel opening (Stefani et al., 1997; Horrigan and Aldrich, 1999), whereas Scheme I requires that channel opening and voltage-sensor movement occur simultaneously.

In the present study, we examine in detail several aspects of mSlo behavior in the absence of Ca^{2+} that deviate from the predictions of Scheme I. The results can be explained by relaxing the assumption that channel opening involves a single concerted voltage-dependent transition. Instead, we suggest that mSlo voltage sensors can move independently and that channel opening and voltage-sensor movement represent distinct events that are allosterically coupled. The resulting model of voltage-dependent gating differs from many common schemes in that the channel can open while any number (or none) of the four voltage sensors are activated. This allosteric mechanism defines a 10-state voltage-gating scheme with multiple open and closed states arranged in parallel, analogous to Scheme I. Similar schemes have been proposed to describe the gating of other voltage-dependent channels (Marks and Jones, 1992; Ríos et al., 1993; McCormack et al., 1994).

The proposed model has important implications for the interpretation and analysis of BK channel structure-function studies because complicated relationships will exist between elementary molecular events such as voltage-sensor movement or channel opening, which give rise to the apparently simple macroscopic features of I_K. In addition, the complexity of the voltage-gating scheme greatly increases the minimum number of states that are required to describe BK channel gating in the presence of Ca^{2+}. Finally, the demonstration that mSlo gating is a multistate process in the absence of Ca^{2+} raises fundamental questions concerning the identity of the step or steps in the activation pathway that are affected by Ca^{2+}.

methods

Channel Expression

Experiments were performed with the mbr5 clone of the mouse homologue of the Slo gene (mSlo), kindly provided by Dr. Larry Salkoff (Washington University School of Medicine, St. Louis, MO). The clone was modified to facilitate mutagenesis and was propagated and cRNA transcribed as previously described (Cox et al., 1997b). *Xenopus* oocytes were injected with ~0.5–5 ng of cRNA (50 nl, 0.01–0.1 ng/nl) 3–7 d before recording.

Electrophysiology

Currents were recorded using the patch clamp technique in the inside out configuration (Hamill et al., 1981). Upon excision, patches were transferred into a separate chamber and washed with at least 20 vol of internal solution. Internal solutions contained (mM): 104 $KMeSO_3$, 6 KCl, and 20 HEPES, and 40 μM (+)-18-crown-6-tetracarboxylic acid (18C6TA) was added to chelate contaminant Ba^{2+} (Diaz et al., 1996; Neyton, 1996; Cox et al., 1997b). In addition "0 Ca^{2+}" solutions contained 2 mM EGTA, reducing free Ca^{2+} to an estimated 0.8 nM based on the presence of ~10 μM contaminant Ca^{2+} (Cox et al., 1997b). 4.5 μM Ca^{2+} solutions were buffered with 1 mM HEDTA and free Ca^{2+} was measured with a Ca^{2+} electrode (Orion Research, Inc.). The external (pipette) solution contained (mM): 108 $KMeSO_3$, 2 KCl, 2 $MgCl_2$, and 20 HEPES. pH was adjusted to 7.2. Experiments were carried out at 5° or 20°C (± ~1°C) as indicated.

Electrodes were made from thick-walled 1010 glass (World Precision Instruments, Inc.) or borosilicate glass (VWR Micropipettes). Their tips were coated with wax (KERR Sticky Wax) and fire polished before use. Pipette access resistance measured in the bath solution (0.5–1.5 MΩ) was used as an estimate of series resistance (R_s) to correct the pipette voltage (V_p) at which I_K was recorded. The corrected pipette voltage, V_m, was used in determining membrane conductance (G_K) from tail current measurements and in plotting the voltage dependence of G_K or the time constant of I_K relaxation [$\tau(I_K)$]. Series resistance error was <15 mV for all data presented and <10 mV for $\tau(I_K)$ measurements.

Data were acquired with an Axopatch 200-B amplifier that was modified to provide an increased voltage range (Axon Instruments) and set in patch mode. Currents were filtered at 100 kHz with the Axopatch's internal four-pole bessel filter and subsequently by an eight-pole bessel filter (Frequency Devices, Inc.). Macroscopic currents were filtered at 30–50 kHz and sampled at 100 kHz with a 16 bit A/D converter (ITC-16; Instrutech Corp.). A P/−4 protocol was used for leak subtraction (Armstrong and Bezanilla, 1974) from a holding potential of −80 mV. To increase the signal to noise ratio, the response to four to eight pulses were typically averaged at each pulse voltage. A Macintosh-based computer system was used in combination with Pulse Control acquisition software (Herrington and Bookman, 1995) and Igor Pro for graphing and data analysis (Wavemetrics Inc.). A Levenberg-Marquardt algorithm was used to perform nonlinear least-squares fits.

Simulations

Simulations were performed using a fifth order Runga-Kutta algorithm with adaptive step size (Press et al., 1992) implemented in Igor Pro (Wavemetrics Inc.).

Filter and Instrumentation Delay

The effect of filtering on I_K activation kinetics was tested by convolving simulated traces that closely match the data with the impulse response of an eight-pole bessel filter. The impulse response was determined as the derivative of the step response, measured for a 2-kHz filter and scaled along the time axis to correspond to a particular corner frequency. Simulations were calculated at 1-μs intervals and were filtered at 100 kHz, and then at 30 kHz to correspond to the experimental arrangement. This procedure introduced a delay of 22 μs, accounting for the majority the instrumentation delay (25 μs), but had no detectable effect on the shape of the simulated traces. Therefore, simulations were left unfiltered and data were corrected for filtering by shifting I_K traces along the time axis by −25 μs. Instrumentation delay was estimated by measuring the time between a voltage step command to the patch clamp and the peak of the capacitive transient (Sigworth and Zhou, 1992).

Single Channel Analysis

Single channel events were observed in patches containing hundreds of channels at voltages where open probability is low ($<10^{-3}$). Currents were typically filtered at 20 kHz, yielding a dead-time of ~10 μs, and were sampled at 50–100 kHz. At voltages where the closed level was clearly defined, total open probability (nP_o) was determined from steady state recordings of 5–45-s duration. All-points amplitude histograms were compiled and the probability (P_k) of occupying each open level (k) was evaluated using a 1/2 amplitude criterion. nP_o was then determined as:

$$nP_o = \sum_k kP_k.$$

nP_o was also evaluated by fitting P_k with a Poisson distribution:

$$P_k = \frac{(nP_o)^k}{k!} e^{-nP_o}.$$

In all cases P_k was well fit by a Poisson distribution and the values of nP_o obtained by the two methods differed by <5%. This is consistent with the idea that I_K represents the activity of a large population of channels with low P_o rather than a subpopulation with higher P_o. Normalized open probability ($P_o/P_{omax} = nP_o/nP_{omax}$) was determined by combining nP_o measurements with an estimate of nP_{omax} obtained from the macroscopic G_K–V relationship in the same patch ($nP_{omax} = G_{Kmax}/g_K$, where g_K is the single channel conductance). Patches that were used to measure single channel activity at negative voltages often produced currents that were too large to measure (>20 nA) at voltages that activate mSlo channels maximally. In these cases, G_{max} was estimated by fitting the macroscopic G_K-V with a Boltzmann function ($\{1 + \exp[-ze(V - V_h)/kT]\}^{-1}$) raised to the 3.2 power as in Fig. 6, B and C.

For voltages >60 mV from the reversal potential (0 mV), single channel amplitudes were large enough that false opening events due to noise were not detected using 20 kHz filtering. The prevalence of false events was assessed by evaluating the number of current transients from the closed level that exceed the 1/2 amplitude criterion in a direction opposite that of the channel opening. nP_o was determined after digitally filtering current records until such false events were not observed at +20 or −20 mV. This procedure yielded a corner frequency of ~5 kHz. For V > +60 mV, no difference in nP_o was observed with 5 or 20 kHz filtering. However, for V < −60 mV, a decrease in nP_o was observed at 5 kHz, reflecting the brevity of open times at these voltages. The largest decreases (~30%) were observed at the most negative voltages (approximately −120 mV). Thus, P_o may be underestimated, but this effect is small when compared with patch-to-patch variation in P_o observed at these voltages (see Fig. 6, E and F).

Shifts in Voltage-dependent Parameters

Patch-to-patch variations in half-activation voltage and other voltage-dependent parameters are observed for mSlo (V_h = 190 ± 10 mV; SD, n = 20 in 0 Ca^{2+}) and hSlo (Stefani et al., 1997), possibly due to differences in redox state of the channel (DiChiara and Reinhart, 1997). Such shifts do not appreciably alter the shape of the G_K-V or other voltage-dependent relationships, but make comparisons of data between different experiments difficult and alter the shape of averaged voltage-dependent relationships relative to those observed in individual experiments. To compensate for this effect, V_h was determined for each patch and compared with the average for all experiments ($\langle V_h \rangle$) at the same [Ca^{2+}]. Data from individual experiments were then shifted along the voltage axis by $\Delta V_h = (\langle V_h \rangle - V_h)$.

results

Delay in I_K Activation

In the absence of Ca^{2+}, mSlo Ca^{2+}-activated K^+ channels open in response to membrane depolarization exhibiting a steady state half-activation voltage of approximately +190 mV (Cox et al., 1997a; Cui et al., 1997). Fig. 1 A_1 shows mSlo I_K evoked in response to a 20-ms pulse to +160 mV from a holding potential of −80 mV in 0 Ca^{2+} (20°C). The time course of activation and deactivation are well fit by exponential functions (Fig. 1 A_1, dashed lines). Similar exponential kinetics are observed over a wide range of voltage and $[Ca^{2+}]_i$ (Cui et al., 1997), suggesting a two-state model with a single voltage-dependent transition between a closed and an open state. However, the exponential activation of I_K is preceded by a brief delay in the presence or absence of Ca^{2+} (Cox et al., 1997a; Stefani et al., 1997). Fig. 1 A_2 shows the initial time course of I_K activation on an expanded time scale. There is a delay of ~100 μs before the current begins to increase, and at least 300 μs is required to achieve an exponential time course (Fig. 1 A_2, dashed line). Although this delay is brief compared with the subsequent relaxation of I_K, it is inconsistent with a two-state gating scheme and suggests that mSlo channels undergo one or more transitions among closed states before opening. To better study these rapid transitions, we examined I_K activation at a reduced temperature. A family of I_K evoked by membrane depolarization at 5°C still exhibits activation kinetics that are well fit by single exponential functions (Fig. 1 B_1). The activation is slowed relative to 20°C, and the delay is similarly prolonged (Fig. 1 B_2). I_K begins to increase after 250 μs and attains an exponential time course after 1 ms. A control trace evoked in response to a voltage pulse to −180 mV is also shown in Fig. 1 B_2; the capaci-

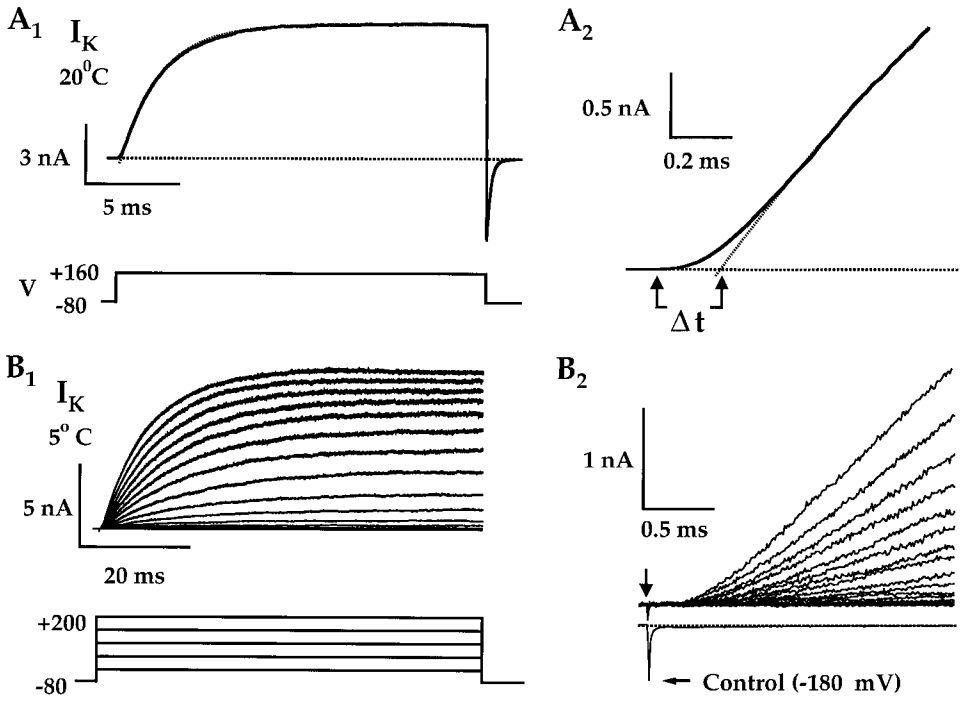

Figure 1. Delay in I_K activation. (A_1) I_K evoked by a voltage pulse to +160 mV from a holding potential of −80 mV at 20°C, representing the average response to 110 pulses. The time course of activation and deactivation are fit by exponential functions (dashed lines). (A_2) The record from A_1 is plotted on an expanded time scale, showing a delay before I_K achieves an exponential time course (dashed line). The delay duration (Δt) is defined as the time where the exponential fit intersects the time axis, and was determined after shifting the I_K trace along the time axis by −25 μs to correct for instrumentation delay (see methods). (B_1) A family of I_K evoked at 5°C in response to 70-ms voltage pulses (+80 to +200 mV in 20-mV steps). Exponential fits (solid lines) are superimposed on the current traces. (B_2) The initial activation of I_K from B_1 exhibits a clear delay. An arrow indicates the start of the voltage pulse. A capacitive transient (control) evoked in response to a pulse to −180 mV was recorded using fast capacity compensation, but no leak subtraction, demonstrating that membrane voltage settles rapidly.

tive transient decays within 30 μs, showing that voltage clamp speed and filter properties contribute little to the delay.

The delay in I_K in the absence of Ca^{2+} indicates that the voltage-dependent activation of mSlo cannot be described by a two-state model. This conclusion is inconsistent with the predictions of Scheme I, where channel opening involves a single concerted step. However, mSlo is a homotetramer and activation is likely to involve the participation of multiple subunits. Unless these subunits move in a strictly concerted manner, channel activation must be described by a multistate scheme that reflects conformational changes in individual subunits. The most extreme deviation from the behavior of a concerted model should occur when subunits act independently (i.e., noncooperatively). Shown below is an example of a completely noncooperative model (Scheme II). This scheme corresponds to that used by Hodgkin and Huxley (1952) to describe the activation of voltage-dependent K^+ channels in squid axon. It assumes that channel opening requires all four identical subunits to undergo independent transitions between a resting (R) and an activated (A) conformation.

$$\begin{matrix} R \underset{\beta}{\overset{\alpha}{\rightleftharpoons}} A \\ R \rightleftharpoons A \\ R \rightleftharpoons A \\ R \rightleftharpoons A \end{matrix} \Big\} O$$

(SCHEME II)

Scheme II can be reduced to a five-state kinetic scheme (Scheme III), where subscripts (0–4) indicate the number of activated subunits in each closed (C) or open (O) state.

$$C_0 \underset{\beta}{\overset{4\alpha}{\rightleftharpoons}} C_1 \underset{2\beta}{\overset{3\alpha}{\rightleftharpoons}} C_2 \underset{3\beta}{\overset{2\alpha}{\rightleftharpoons}} C_3 \underset{4\beta}{\overset{\alpha}{\rightleftharpoons}} O_4$$

(SCHEME III)

Scheme III predicts a delay, but it cannot reproduce the kinetics of mSlo activation. The Hodgkin-Huxley model produces an activation time course that is highly sigmoidal because the delay and subsequent activation of I_K are both determined by a single process (subunit activation) and therefore occur on a similar time scale. When Scheme III is fit to the brief delay in mSlo I_K, it predicts an activation time course that is too rapid (Fig. 2, A_1 and A_2).

The relationship between the delay and subsequent relaxation of I_K can be defined precisely for models like Scheme II, which require *n* independent subunits to be activated before channels are open (Hodgkin and Huxley, 1952; Cole and Moore, 1960; Colquhoun and Hawkes, 1977). For such models, the time-dependent occupancy of the open state is:

$$O(t) = [A(t)]^n, \quad (1)$$

where $A(t)$ represents the probability that a subunit is activated:

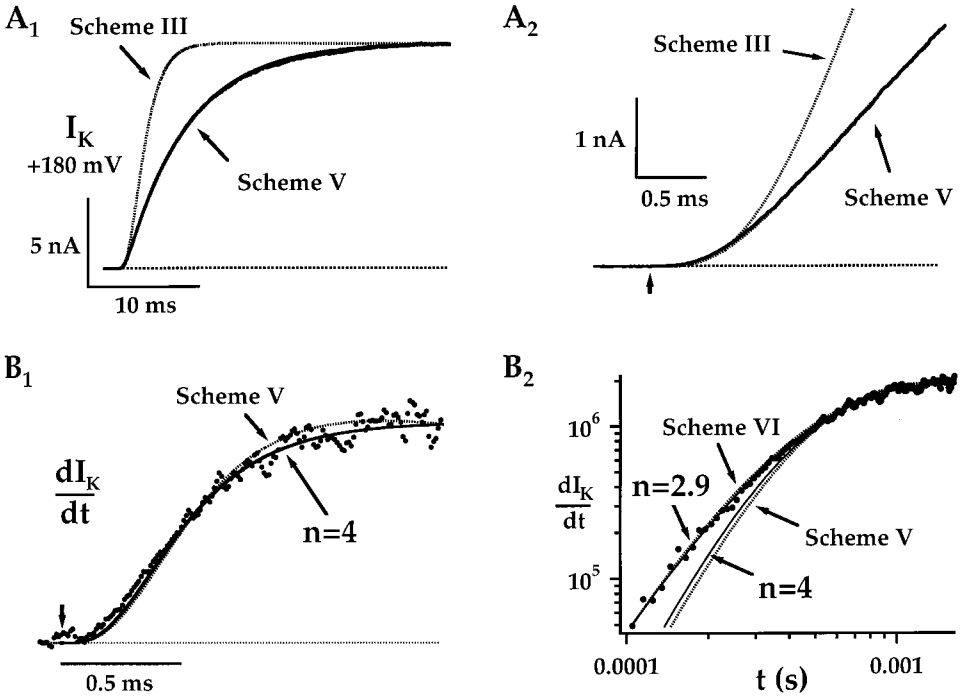

Figure 2. Kinetics of I_K delay. (A_1) I_K evoked at +180 mV (7°C) is compared with the prediction of a Hodgkin-Huxley model (Scheme III: $\alpha = 375\ s^{-1}$, $\beta = 660\ s^{-1}$) that approximates the delay in I_K (A_2), but does not reproduce the subsequent time course of activation. Scheme V fits both the delay and activation time course ($\alpha = 2{,}018\ s^{-1}$, $\beta = 1{,}172\ s^{-1}$, $\delta = 341\ s^{-1}$, $\gamma = 136\ s^{-1}$). Both models were constrained to reproduce the steady state open probability measured at the end of the pulse ($P_o \cong G_K/G_{Kmax} = 0.29$) and assume channels occupy the first closed state (C_0) at the start of the pulse. The derivative of the trace in A [$d(I_K)/dt$] is plotted on linear (B_1) and log–log (B_2) scales and is fit by a function $(1 - e^{-t/\tau})^n$, where $n = 4$ and $\tau = 270\ \mu s$ (B_1 and B_2, solid line). A better fit is obtained with $n = 2.9$ and $\tau = 316\ \mu s$ (B_2, solid line). The predictions of sequential gating Schemes V and VI are indicated by dashed lines. (Scheme VI: X = 3, $\alpha = 600\ s^{-1}$, $\beta = 349\ s^{-1}$, $\delta = 341\ s^{-1}$, $\gamma = 136\ s^{-1}$). Current traces were shifted along the time axis by −25 μs to correct for the instrumentation delay (see methods).

$$A(t) = A_\infty(1 - e^{-t/\tau}) \tag{2}$$

and $\tau = 1/(\alpha + \beta)$ is the time constant of subunit activation, with $A_\infty = \alpha/(\alpha + \beta)$ representing the steady state activation. The time course of I_K activation is determined by combining Eqs. 1 and 2 and expanding in a binomial series:

$$I_K = I_\infty(1 - e^{-t/\tau})^n = I_\infty \sum_{k=0}^{n} \frac{(-1)^k n!}{k!(n-k)} e^{-kt/\tau}, \tag{3}$$

where I_∞ is proportional to $A_\infty{}^n$ and represents the steady state amplitude of I_K. The delay duration (Δt) is defined by fitting the slowest component of I_K relaxation after the delay (I_{slow}) with a single exponential function:

$$I_{slow} = I_\infty(1 - e^{(\Delta t - t)/\tau}). \tag{4}$$

This function intersects the time axis at $t = \Delta t$. I_{slow} can be determined from the first two terms of the series in Eq. 3:

$$I_{slow} = I_\infty(1 - ne^{-t/\tau}). \tag{5}$$

Combining Eqs. 4 and 5:

$$\Delta t = \ln(n)\tau. \tag{6}$$

For a Hodgkin-Huxley model ($n = 4$), $\Delta t = 1.39\ \tau(I_K)$ represents the slow time constant of I_K relaxation. In contrast, the data in Fig. 2 A indicate $\Delta t = 0.12\ \gamma(I_K)$.

The rapid attainment of an exponential time course in Fig. 2 A suggests that the transitions responsible for the delay equilibrate within 1 ms and that a much slower process limits activation during the subsequent 30 ms. Scheme II can reproduce such behavior only when subunits interact in a highly negatively cooperative manner such that one transition becomes rate limiting while others equilibrate rapidly. An alternative model (Scheme IV) can account for I_K kinetics with the assumption that subunits undergo rapid independent transitions, as in Scheme II, but that channel opening involves an additional conformational change that is slow and rate limiting (Ledwell and Aldrich, 1999).

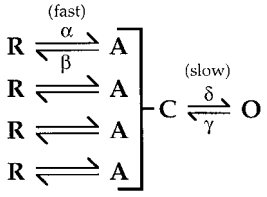

(SCHEME IV)

If channel opening can only occur when all four subunits are activated, this model reduces to a six-state kinetic scheme (Scheme V). Scheme V assumes that subunits undergo independent conformational changes

when the channel is closed. However, the overall activation scheme is cooperative because the final transition from C to O depends on the state of all four subunits, which requires that they interact (Wyman and Gill, 1990; Sigworth, 1994; Zagotta et al., 1994a).

$$C_0 \underset{\beta}{\overset{4\alpha}{\rightleftharpoons}} C_1 \underset{2\beta}{\overset{3\alpha}{\rightleftharpoons}} C_2 \underset{3\beta}{\overset{2\alpha}{\rightleftharpoons}} C_3 \underset{4\beta}{\overset{\alpha}{\rightleftharpoons}} C_4 \underset{\gamma}{\overset{\delta}{\rightleftharpoons}} O_4$$

(SCHEME V)

Scheme V provides a reasonable fit to both the brief delay and exponential activation time course of I_K at +180 mV (Fig. 2 A). To test this model in more detail, we analyzed the delay kinetics. Models like Scheme V, which require n independent subunits to be activated before channels can open, predict I_K kinetics more complex than predicted by Eq. 3. However, the rate of I_K activation ($I_K'(t) = dI_K/dt$) during the delay can be approximated by the expression:

$$I'_K(t) = I'_{Kmax}[1 - e^{-t/\tau}]^n, \quad (7)$$

provided two conditions are satisfied. First, subunit activation must be much faster than the C–O transition. The relative kinetics of the delay and I_K relaxation suggest this is the case for mSlo. Second, few channels must occupy the open state. This is satisfied during the delay in I_K activation because I_K achieves an exponential time course when P_o, estimated from G_K/G_{Kmax}, is <0.05. Given these assumptions, the time-dependent occupancy of the last closed state (C_L) is determined primarily by transitions among closed states and can be approximated:

$$C_L(t) = [A(t)]^n, \quad (8)$$

The rate of change in occupancy of the open state ($O'(t) = dO/dt$) is then:

$$O'(t) = \delta C_L(t) - \gamma O(t). \quad (9)$$

When few channels are open, such that $\gamma O << \delta C_L$, this expression simplifies to:

$$O'(t) = \delta C_L(t). \quad (10)$$

The expression for $I'_K(t)$ (Eq. 7) is then determined by combining Eqs. 2, 8, and 10.

Fig. 2 A_2 shows the initial time course of I_K at +180 mV; the time derivative of this record is plotted on linear (Fig. 2 B_1) and log–log (B_2) scales. The time course of $I'_K(t)$ is sigmoidal, and can be approximated by Scheme V or by Eq. 7 with $n = 4$ (Fig. 2, B_1 and B_2). However, the log–log plot reveals that I'_K is best fit when n is reduced to 2.9 (Fig. 2 B_2). This deviation from the prediction of Scheme V is small, but significant, and suggests that a more complicated model may be necessary to explain our results. One way to fit the data is by modifying Scheme V to include direct cooperative interactions between subunits. For example, Scheme VI assumes that the forward and backward rate constants for subunit activation are increased by a factor X for each subunit that is in the activated state.

$$C_0 \underset{\beta}{\overset{4\alpha}{\rightleftharpoons}} C_1 \underset{2\beta X}{\overset{3\alpha X}{\rightleftharpoons}} C_2 \underset{3\beta X^2}{\overset{2\alpha X^2}{\rightleftharpoons}} C_3 \underset{4\beta X^3}{\overset{\alpha X^3}{\rightleftharpoons}} C_4 \underset{\gamma}{\overset{\delta}{\rightleftharpoons}} O_4$$

(SCHEME VI)

The equilibrium properties of Schemes V and VI are identical, but Scheme VI can fit $I'_K(t)$ with X = 3 (Fig. 2 B_2). Similar results are obtained if only the forward rate is effected by subunit activation, thereby altering the equilibrium constants (X = 3.5, data not shown). However, our most favored model, discussed later, can account for these results without abandoning the idea that subunits undergo independent transitions.

Several experimental factors might contribute to a deviation between I_K kinetics and the prediction of Scheme V. The membrane charging time constant for an excised patch is expected to be very fast ($\tau = C_m R_s \leq$ 1 μs, see methods) and should not affect I_K kinetics. The relaxation of the capacitive transient in Fig. 1 B_2 (control) is mainly limited by the filtering of the current signal. To test whether filtering affects I_K kinetics, simulated traces in Fig. 2 were convolved with the impulse responses of 100- and 30-kHz eight-pole bessel filters to reproduce experimental conditions (see methods). The filtered and unfiltered traces were indistinguishable after compensating for a 22-μs filter delay (data not shown). Thus, I_K kinetics are not modified by filtering and appear to represent a genuine property of the channel.

It is conceivable that Scheme V could give rise to the observed delay kinetics if channels were distributed in states other than C_0 at the start of the voltage pulse. This possibility was ruled out by examining the effect of initial conditions on the delay. Fig. 3 A shows the time course of I_K evoked at +180 mV after a 1-ms prepulse to voltages between −80 and +120 mV. Prepulses to voltages >0 mV produced a progressive decrease in the delay, resulting in a shift of I_K along the time axis analogous to that reported by Cole and Moore (1960) for K^+ current in squid axon. A similar effect was reported for hSlo channels by Stefani et al. (1997). This Cole-Moore shift indicates that the initial distribution of channels among closed states is voltage dependent. However,

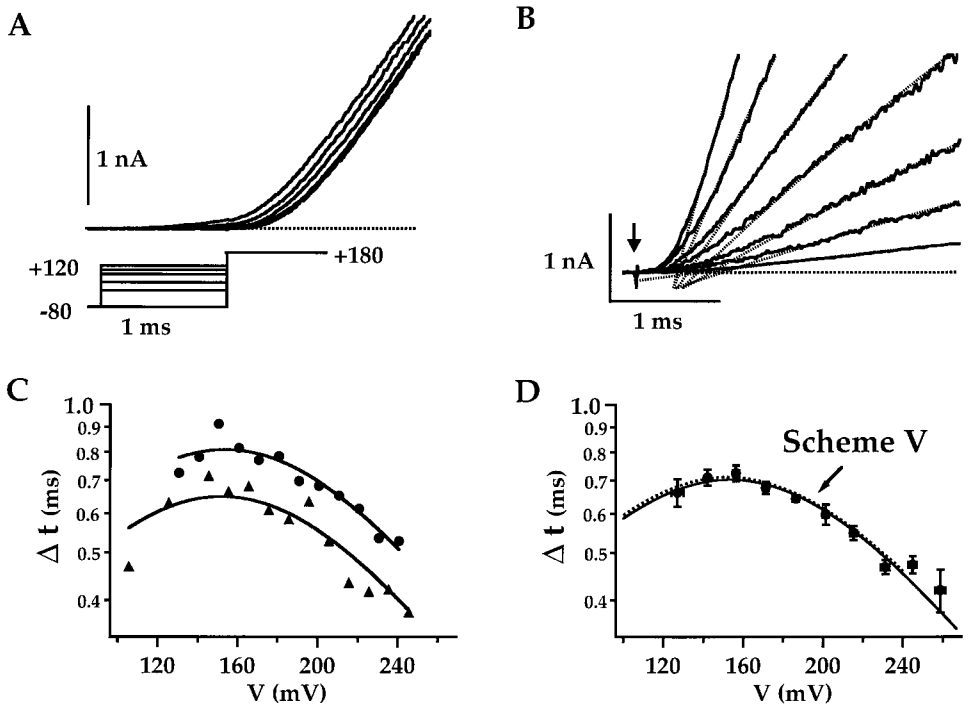

Figure 3. Voltage dependence of I_K delay. (A) The initial time course of I_K activation measured at +180 mV from the same patch as Fig. 2 shows a decreased delay following a 1-ms prepulse to various voltages (−80, 0, 40, 80, 100, and 120 mV). To accurately represent the time course of channel opening, currents during the prepulse were scaled by a factor $I_K(+180)/I_K(V_{pre})$ representing the ratio of single channel current amplitudes measured at the test and prepulse voltages. (B) A family of I_K evoked at different voltages (+120 to +240 in 20-mV steps, holding potential = −80) are fit with exponential functions (dashed lines), demonstrating a voltage-dependent change in delay. (C) Delay duration (Δt) is plotted versus pulse voltage for two experiments. The plots are fit by functions of the form $\Delta t = 1/(a + b)$ with $a = a_o * e^{(z_a e/kt)}$, $b = b_o * e^{(z_b e/kt)}$ ($z_a = +0.28\ e$, $z_b = -0.28\ e$; (▲) $a_o = 124\ s^{-1}$, $b_o = 4{,}767\ s^{-1}$; (●) $a_o = 98\ s^{-1}$, $b_o = 3{,}902\ s^{-1}$). The delay was not well determined at the lowest voltages; therefore, fits were constrained with the simplifying assumption $z_a = z_b$. (D) The average Δt–V relationship (mean ± SEM, $n = 6$), was obtained after first normalizing individual plots (see text) to mean Δt measured from +180 to +195 mV. The data are fit by the above function (solid line, $z_a = +0.28\ e$; $z_b = -0.28\ e$; $a_o = 119\ s^{-1}$, $b_o = 4{,}240\ s^{-1}$) and reproduced by Scheme V [dashed line: $z_\alpha = +0.28\ e$, $\alpha(0) = 244\ s^{-1}$, $z_\beta = -0.28\ e$, $\beta(0) = 8{,}670\ s^{-1}$, $z_\delta = 0.155\ e$, $\delta(0) = 49.4\ s^{-1}$, $z_\gamma = -0.155\ e$, $\gamma(0) = 134\ s^{-1}$]. The rate constants in Scheme V that describe voltage sensor movement (α, β) are 2.05-fold greater than (a, b) at all voltages. Thus $\Delta t = 1/(a + b)$ is proportional the voltage-sensor time constant $\tau = 1/(\alpha + \beta)$. The parameters that describe the C–O transition in Scheme V (δ, z_δ, γ, z_γ), were adjusted to fit the P_o–V relationship (see Fig. 6 B) and to reproduce the time course of I_K activation at the peak of the Δt–V relationship (+153 mV).

prepulses to −80 or 0 mV had no detectable effect on the delay, suggesting that the closed state distribution does not change at voltages <0 mV. This result supports the assumption that channels mainly occupy the ground state (C_0) at −80 mV.

Voltage Dependence of the Delay in I_K Activation

Although the delay kinetics deviate from the prediction of Scheme V, they are consistent with the idea that multiple closed-state transitions precede channel opening. In addition, the dependence of the delay on prepulse voltage implies that closed-state transitions are voltage dependent. To help characterize the voltage dependence of these early transitions, we measured the delay duration (Δt) during pulses to different voltages. Δt was determined by fitting I_K with exponential functions (Eq. 4), as shown in Fig. 3 B. Fig. 3 C plots Δt on a log scale versus pulse voltage for two different experiments. The average Δt–V relationship is plotted in Fig. 3 D (mean ± SEM, $n = 6$). The delay is maximal at approximately +155 mV and exhibits a bell-shaped voltage dependence.

The two Δt–V relationships in Fig. 3 C are similar in shape but differ in magnitude by ~25%, possibly reflecting variations in temperature (T = 5 ± 1°C) (Δt has a Q_{10} of 2.3 based on comparison of the delay at 20°C in Fig. 1 B (210 μs) to the mean delay measured at 5°C (725 μs) at +160 mV). To compensate for patch-to-patch variation in the magnitude of Δt, the average Δt–V relationship in Fig. 3 D was determined after first normalizing the component Δt–V's to the mean Δt at +180–195 mV. The ability of the average and individual relationships to be fit by the same functions (Fig. 3, C and D, solid lines), discussed below, argues that the average accurately captures the shape of the Δt–V.

In general, the relationship between the Δt and the kinetics of closed-state transitions will not be as simple as described for Scheme II (Eq. 6). The time course of I_K, and therefore the delay duration, may be influenced by transitions between closed and open states and by O–O transitions if multiple open states exist. Previous

studies of *Shaker* K^+ channels have taken the approach of measuring delay duration at high voltages to estimate the kinetics of closed-state transitions (Zagotta et al., 1994b; Schoppa and Sigworth, 1998a). At sufficiently positive voltages, the backward rate constant from open to closed is assumed to be small such that the occupancy of the open state reflects only the rate of leaving the closed state. In other words, the time course of I_K approximates the cumulative distribution of latencies to first opening, and Δt is highly dependent upon closed-state transition kinetics.

In this study, Δt was measured over a range of voltages where backward rate constants from open to closed may not be negligible. However, the initial time course of $I'_K(t)$ during the delay should be determined mainly by the rate of leaving the closed state when P_o is small (Eq. 10). Thus, the initial time course of I_K and the delay duration will be determined by closed-state transition kinetics provided I_K achieves an exponential time course while P_o is small. This condition appears to be satisfied at all voltages where Δt was measured for mSlo (see Figs. 1 B_1 and 3 B). Therefore, the Δt–V relationship should provide information about the voltage dependence of closed state transitions. Such an argument cannot be made in the case of *Shaker* K^+ channels because the time course of activation has pronounced sigmoidicity such that P_o is not small when I_K achieves an exponential time course.

The precise relationship between closed-state transition kinetics and Δt is model dependent. For some models, including Scheme V, Δt will be proportional to the time constant of voltage sensor movement τ_J (provided I_K achieves an exponential time course when P_o is small and transitions among closed states are fast relative to channel opening); in which case, the Δt–V relationship can be used to determine the voltage dependence of the R–A transition (see appendix).

Consistent with the prediction that Δt reflects the voltage dependence of τ_J, the Δt–V relations can be fit by functions of the form $\Delta t = 1/(a + b)$, where $a = a_o * e^{(z_a e/kT)}$, $b = b_o * e^{(-z_b e/kT)}$ ($z_a = z_b = 0.28\ e$) (Fig. 3, C and D, solid lines). The bell-shaped voltage dependence is consistent with a process governed by a single transition with voltage-dependent forward and backward rate constants. If Δt is proportional to $\tau_J[v]$ then $z_a = z_\alpha$ and $z_b = z_\beta$, and the fit to the average Δt–V relationship in Fig. 3 D implies that the transition from R to A involves a total charge movement ($z_J = z_\alpha + z_\beta$) of 0.56 e with a half-activation voltage (V_h) of +153 mV, corresponding to the peak of the Δt–V. Simulations of Scheme V using these parameters can reproduce the Δt–V relationship (Fig. 3 D, dashed line). Although our final model is more complicated than Scheme V, we show later that it can reproduce the Δt–V relationship using similar parameters for the voltage-sensor transition ($z_J = 0.55\ e$, $V_h = +145$ mV). Moreover, gating current measurements in the companion article produce similar results ($z_J = 0.55\ e$, $V_h = +155$ mV) (Horrigan and Aldrich, 1999). Thus measurements of I_K delay appear to provide a reasonable method for characterizing mSlo voltage-sensor movement.

The Voltage Dependence of I_K Relaxation

The predominantly exponential time course of I_K suggests that mSlo activation is dominated by a single rate-limiting step. To study the properties of this transition, we examined the voltage dependence of I_K relaxation kinetics. The time constant of I_K relaxation, measured after the delay, changes with voltage, suggesting that the rate-limiting step may be voltage dependent (Cox et al., 1997a). But mSlo gating is a multistate process with rapid, voltage-dependent transitions among closed states. While the kinetics of closed-state transitions are too fast to limit the exponential relaxation of I_K, $\tau(I_K)$ may be influenced by the equilibrium distribution of closed states. Therefore, the voltage dependence of $\tau(I_K)$ may reflect a voltage dependence of the closed-state equilibria in addition to the rate-limiting step. For example, Scheme V predicts:

$$\tau(I_K) = \frac{1}{\delta PC_L + \gamma}, \qquad (11)$$

where PC_L represents the conditional probability that a closed channel occupies the last closed state [i.e., $P(C_4|C)$ for Scheme V]. Eq. 11 is valid for any scheme with a single open state and a single closed–open transition, provided the C–O transition is rate limiting and the preceding C–C transitions are equilibrated. Although Eq. 11 contains a voltage-dependent contribution from closed-state equilibria (PC_L), at extreme voltages, $\tau(I_K)$ depends only on the rate-limiting step. For example, at negative voltages where PC_L is small, $\tau(I_K) = 1/\gamma$, at positive voltages where $PC_L = 1$ and $\delta >> \gamma$, $\tau(I_K) = 1/\delta$. Even if PC_L fails to achieve limiting values of 0 or 1, the voltage dependence of $\tau(I_K)$ at extreme voltages should reflect only the voltage dependence of δ or γ, provided PC_L is relatively constant.

The voltage dependence of $\tau(I_K)$ was examined in an experiment illustrated in Fig. 4. I_K was activated by stepping from a holding potential of −80 mV to voltages between +100 and +240 mV (Fig. 4 A). I_K tail currents were recorded at more negative voltages, following a 50-ms depolarization to +120 mV (Fig. 4, B–D). In all cases, the time course of I_K was well fit by an exponential function after a brief delay (Fig. 4, solid lines). $\tau(I_K)$ is plotted from +30 to +240 mV in Fig. 5 A and exhibits a bell-shaped voltage dependence that can be fit by a two-state model (solid curve) (Cui et al., 1997). This behavior also appears consistent with the prediction of

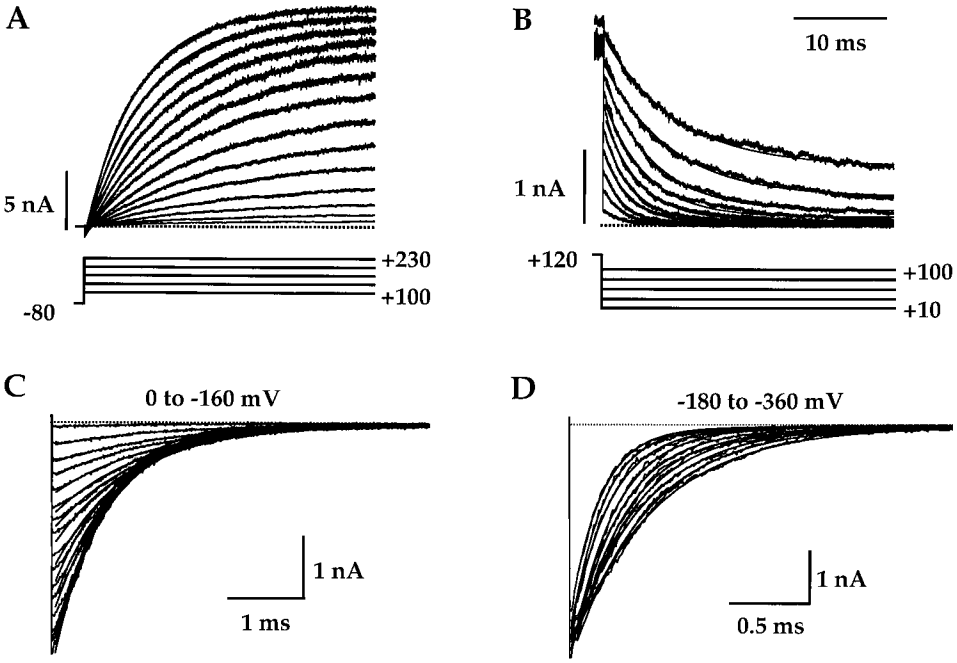

Figure 4. The voltage-dependence of I_K relaxation. (A) Activation and (B–D) deactivation kinetics measured at 5°C are fit by exponential functions (solid lines). I_K was activated in response to voltages from +100 to +240 mV. Deactivation was measured at the indicated voltages after a 50-ms depolarization to +120 mV.

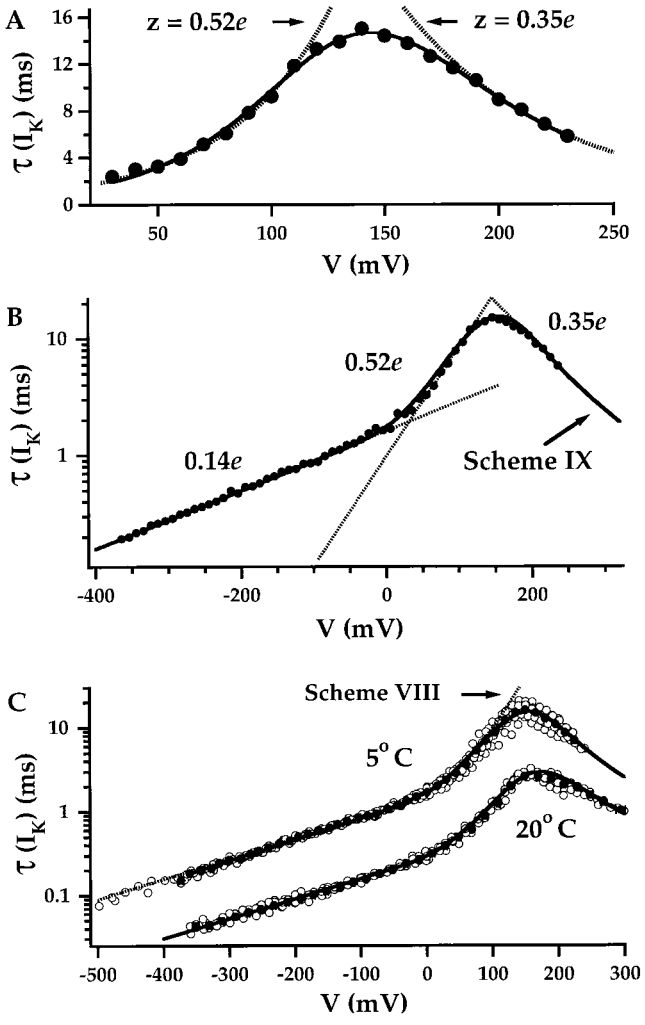

Scheme V because $\tau(I_K)$ increases exponentially with voltage from +30 to +110 mV and decreases exponentially from +180 to +240 (Fig. 5 A, dashed lines) as if $\tau(I_K)$ is determined by single voltage-dependent rate constants at these voltages. However, our analysis of the delay in I_K activation suggests that the voltage range in Fig. 5 A is insufficient to observe the limiting voltage dependence of $\tau(I_K)$. The Cole-Moore shift (Fig. 3 A) indicates that closed-state equilibria change from +40 to +120 mV, and the weak voltage dependence of the delay (Fig. 3 C) suggests that these equilibria continue to change over a large voltage range.

To test the limiting behavior of $\tau(I_K)$, tail currents were measured at very negative voltages (Fig. 4, C and D). Fig. 5 B plots $\tau(I_K)$ for the data in Fig. 4 down to

Figure 5. The voltage dependence of $\tau(I_K)$. (A) Time constants [$\tau(I_K)$] from the fits in Fig. 4, A and B, are plotted versus voltage and fit (dashed line) by two exponential functions with the indicated equivalent charge (z). The prediction of a two-state model [$\tau(I_K) = 1/(a + b)$, $a = a_o * e^{(z_a e/kt)}$, $b = b_o * e^{(z_b e/kt)}$] is indicated by a solid line ($z_a = 0.37\ e$, $z_b = 0.67\ e$; $a_o = 4.86\ s^{-1}$, $b_o = 1{,}323\ s^{-1}$). (B) $\tau(I_K)$ is plotted on a log scale versus voltage for all the records in Fig. 4. Data were shifted along the voltage axis by $\Delta V_h = +5.6$ mV (see methods). Three regions of exponential voltage dependence are shown by dashed lines with the indicated equivalent charges (z). A solid curve indicates a fit to Scheme IX (Table I, Patch 1). (C) $\tau(I_K)$–V plots obtained from multiple experiments at 5° and 20°C (○) were normalized to mean $\tau(I_K)$ at −80 mV, and then averaged in 15-mV bins (●). Solid curves indicate fits of Scheme IX to the averaged data (Table I: average 5° and 20°C). The dashed curve represents a fit of Scheme VIII to the average 5°C data for V < +100 mV ($z_{\beta 1} = -0.45\ e$, $\beta_1(0) = 2{,}400\ s^{-1}$, $z_{\beta 2} = -0.14\ e$, $\beta_2(0) = 700\ s^{-1}$, $z_{\alpha 2} = -0.26\ e$, $\alpha_2(0) = 300\ s^{-1}$).

TABLE I

Scheme IX Kinetic Parameters

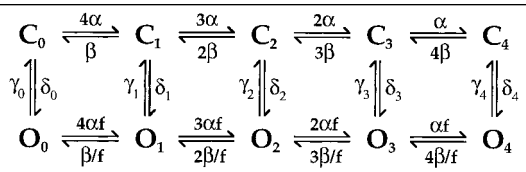

Parameters	Patch 1	Patch 2	Average 5°C	Average 20°C
	s^{-1}	s^{-1}	s^{-1}	s^{-1}
$\alpha(0)$*	276	257	238	1276
$\beta(0)$	7650	7129	6596	35370
$\delta_0(0)$*	0.00128	0.00384	0.00138	0.0074
$\delta_1(0)$*	0.0218	0.0653	0.0235	0.126
$\delta_2(0)$*	0.370	1.11	0.399	2.14
$\delta_3(0)$*	2.27	6.99	2.51	25.7
$\delta_4(0)$*	16.4	44.0	15.8	49.3
$\gamma_0(0)$	640	1923	690	3700
$\gamma_1(0)$	640	1923	690	3700
$\gamma_2(0)$	640	1923	690	3700
$\gamma_3(0)$	269	712	256	2612
$\gamma_4(0)$	98.3	294	94.8	295

*These rate constants in combination with the following parameters are sufficient to define the kinetic behavior of the model ($z_\alpha = +0.275\ e$, $z_\beta = -0.275\ e$, $z_\delta = +0.262\ e$, $z_\gamma = -0.138\ e$, $D = 17$, $f = \sqrt{D}$, $[\delta_0(0)/\gamma_0(0)] = L(0) = 2\ e^{-6}$, $\alpha/\beta = J = 1$ at +145 mV [$V_h(J)$].

−360 mV and, in other experiments, $\tau(I_K)$ was measured at voltages as low as −500 mV (Fig. 5 C). Tail currents were always well fit by exponential functions, but the $\tau(I_K)$–V relationship at negative voltages departs from that observed in Fig. 5 A. For $V < +30$ mV, the slope of the $\tau(I_K)$–V relationship decreases and achieves an exponential voltage dependence of only e-fold per 170 mV (0.14 *e* equivalent charge) from −360 to −40 mV. Fits to $\tau(I_K)$–V in Fig. 5 B define three regions of exponential voltage dependence, characterized by mean equivalent charges of $+0.143\ e \pm 0.003$, $+0.49\ e \pm 0.02$, and $-0.29\ e \pm 0.02$ (mean ± SEM, $n = 5$) over voltage ranges of −500 to −20 mV, +30 to +140 mV, and +180 to +280 mV, respectively.

A similar voltage dependence is observed at 20° and 5°C (Fig. 5 C). The individual plots were normalized to the average time constants measured at −80 mV for 5°C (0.95 ± 0.04 ms, $n = 6$) or 20°C (0.172 ± 0.015 ms, $n = 6$). The increase in temperature speeds I_K relaxation 5.5-fold at all voltages ($Q_{10} = 3.1$) such that the shape of the $\tau(I_K)$–V is essentially unchanged. This also demonstrates that measurements of the $\tau(I_K)$–V relationship at negative voltages at 5°C are not limited by our ability to resolve fast tail currents. Nor is the limiting voltage dependence affected by series resistance error because tail current amplitudes saturate at voltages less than −150 mV (Fig. 4 D). In this experiment, the tail current amplitude was <5 nA at even the most negative voltages, the electrode resistance was 1 MΩ, and the series resistance error was ~5 mV or less and constant from −150 to −360 mV.

The $\tau(I_K)$–V relationship at negative voltages is likely to represent the limiting behavior of $\tau(I_K)$ since no deviation from exponential voltage dependence was observed down to −500 mV (Fig. 5 C). Unfortunately, the voltage dependence of $\tau(I_K)$ could not be tested at very positive voltages. Recordings of I_K at extreme negative voltages were possible because tail currents decayed rapidly and the time spent at these voltages could therefore be minimized (e.g., 0.5 ms at −500 mV). Measuring the slower time course of I_K activation required longer voltage pulses (≥10 ms, 5°C), which tends to compromise patch stability above +300 mV. Shorter pulses can be used at 20°C because activation is faster, but higher temperatures also tended to reduce patch stability and thereby offset the benefit of reduced pulse duration.

Scheme V predicts that $\tau(I_K)$ should achieve a limiting exponential voltage dependence, but the $\tau(I_K)$–V relationship is inconsistent with this model. According to Scheme V, $\tau(I_K) = 1/\gamma$ at negative voltages, and the exponential relationship defined by $\tau(I_K)$–V between −360 and −40 mV in Fig. 5 B ($\tau_{Lim(-)}$) should represent $1/\gamma$. However, Scheme V also requires that $\tau(I_K)$ satisfy the inequality $\tau(I_K) \leq 1/\gamma$ at all voltages because ($\delta\ PC_L + \gamma$) ≥ γ (Eq. 11). The data clearly do not meet this condition because $\tau(I_K)$ measured from +10 to +230 mV is up to fivefold greater than $\tau_{Lim(-)}$ (Fig. 5 B).

The complex voltage dependence of $\tau(I_K)$ could be accounted for by a sequential gating scheme that, unlike Scheme V, contains multiple rate-limiting transitions. In general, the relaxation of any system of *n* states will be multiexponential with $n - 1$ characteristic time constants. In Scheme V, all but one of these time constants is fast and relaxes during the delay in I_K activation. The remaining slow time constant, reflecting the C–O transition, dominates the time course of I_K relaxation, and the voltage dependence of $\tau(I_K)$ exhibits two regions of exponential voltage dependence associated with the forward and backward rate constants for this transition. If additional transitions in the activation pathway were slow, then they could also limit the time course of I_K relaxation over some voltage range, possibly contributing additional regions of exponential voltage dependence to the $\tau(I_K)$–V relationship.

A sequential scheme containing multiple rate limiting transitions cannot be ruled out based on the data presented thus far. However such a model is difficult to reconcile with the observation that I_K relaxes with a predominantly single exponential time course at all voltages. The problem can be illustrated by attempting

to fit the $\tau(I_K)$–V with a general sequential scheme containing a single open state (Scheme VII).

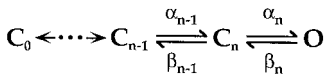

(SCHEME VII)

We will restrict our analysis to voltages less than +100 mV where steady state open probability is small ($<10^{-2}$), and consider the case where channels begin in the open state (i.e., tail currents). For Scheme VII, as for Scheme V, $\tau(I_K)$ is determined at negative voltages by the rate of leaving O [$\tau(I_K) = \tau_{Lim(-)} = 1/\beta_n$]. Under what conditions will I_K relax with $\tau(I_K) > 1/\beta_n$, as observed at more positive voltages? First, $\tau(I_K)$ can differ from $1/\beta_n$ only when $\alpha_n > 0$. Moreover, α_n must be large compared with β_n for I_K to relax with an exponential time course. To see this, consider the relaxation of I_K at +100 mV where $\tau(I_K)$ is approximately fourfold greater than $\tau_{Lim(-)}$ (Fig. 5 B). If I_K is described by a single exponential function with $\tau(I_K) = 4\tau_{Lim(-)} = 4/\beta_n$, then:

$$O'(t) = \left(\frac{-\beta_n}{4}\right)O(t). \quad (12)$$

When $O(0) = 1$, the initial rate of I_K decay is given by $O'(0) = -\beta_n/4$, but the general scheme (Scheme VII) predicts a much faster initial decay $O'(0) = -\beta_n$, as required by the expression:

$$O'(t) = \alpha_n C_n(t) - \beta_n O(t). \quad (13)$$

Hence there must exist a fast component of I_K relaxation that is not evident in the data.

If the amplitude of the fast component is small, then, after it decays, Eq. 13 should be approximated by Eq. 12. Equating Eqs. 12 and 13 gives:

$$\alpha_n = 0.75\ \beta_n\left[\frac{O(t)}{C_n(t)}\right]. \quad (14)$$

If $O(t)$ is still large after the fast component has decayed, then $[O(t)/C_n(t)]$ will be large, implying $\alpha_n >> \beta_n$, and the final equilibrium constant for the C–O transition will be large ($\alpha_n/\beta_n >> 1$) even when P_o is small ($<10^{-2}$), which suggests that some other forward rate constant in the activation scheme is small at +100 mV. If α_{n-1} is very small when V < +100 mV, then Scheme VII can be approximated by a three-state model (Scheme VIII), which can be solved exactly and is characterized by two time constants: τ_{slow} and τ_{fast}.

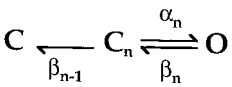

(SCHEME VIII)

The dashed line in Fig. 5 C shows that this scheme can fit the $\tau(I_K)$–V relationship at 5°C (for V ≤ +100 mV). Using the parameters in the figure legend, $\tau(I_K)$ is equal to τ_{slow}, and τ_{fast} will be at least 4.5× smaller than τ_{slow}. Such a fast component would be observable if its amplitude were significant, but the amplitude of the fast component was adjusted to <20% of the total by requiring α_n/β_n to be large ($\alpha_n/\beta_n = 2.1$ at +100 mV). Thus the fast component can be made small, giving the appearance of a monoexponential decay.

That is, a general sequential scheme (Scheme VII), whose final C to O transition is not rate limiting, can reproduce important features of the $\tau(I_K)$–V relationship while maintaining a predominantly exponential relaxation time course. We can not exclude that a minor fast component of tail current relaxation exists. Furthermore, the requirement that the final C–O transition is faster than some closed-state transitions is not in conflict with the observation of a brief delay in I_K activation (Schoppa and Sigworth, 1998a). However, mSlo gating currents described in the companion article (Horrigan and Aldrich, 1999) activate without a detectable rising phase and decay rapidly compared with $\tau(I_K)$, supporting the idea that the initial closed-state transitions are fast and voltage dependent. Furthermore, a large fraction of gating charge moves at voltages where the steady state P_o is small, implying that intermediate closed states are occupied under these conditions. Thus, to account for both exponential I_K kinetics and a low P_o at +100 mV, the general sequential scheme would require that an intermediate closed-state transition is slow. Such a model is difficult to describe in terms of only two molecular events: channel opening and subunit activation. However an alternative scheme, presented below, can be described in these simple molecular terms while accounting for the $\tau(I_K)$–V relationship and generating exponential kinetics.

An Allosteric Model of Voltage-dependent Gating

Although the $\tau(I_K)$–V relationship is inconsistent with Scheme V, the data can be explained in terms of the conformational events outlined in Scheme IV. If mSlo channels can open even when one or more subunits are in the R conformation, Scheme IV can be represented by a 10-state gating scheme with 5 open and 5 closed states (Scheme IX), where each horizontal transition (C–C or O–O) represents a subunit conformational change, and vertical transitions represent channel opening.

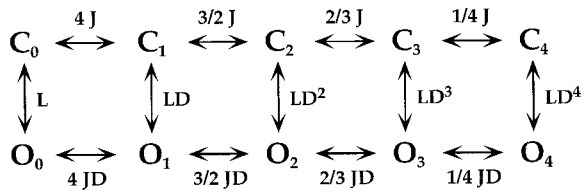

(SCHEME IX)

As before, subscripts (0–4) denote the number of activated subunits in each open and closed state. Scheme IX predicts that channels can open even if no subunits are activated (C_0–O_0). However, such an event should be rare because subunit activation is assumed to increase the probability of channel opening. This interaction is represented by a factor D. The equilibrium constants for the C–O transitions increase D-fold for each subunit that is activated. As will be shown later, this requirement favors the possibility that channels will pass through several closed states before opening in response to a voltage step, consistent with the presence of a delay in I_K activation. In addition, if the C–O transitions are slow and rate limiting, while C–C and O–O transitions equilibrate rapidly, this model can account for I_K kinetics that are essentially exponential after the delay at all voltages. At the same time, Scheme IX can reproduce the complex voltage dependence of $\tau(I_K)$ because it contains multiple rate-limiting C–O transitions that dominate I_K relaxation over different voltage ranges. Both the individual and average $\tau(I_K)$–V relationships in Fig. 5, B and C, are well (solid curves) fit by Scheme IX. The observation that a change in temperature has little effect on the shape of the $\tau(I_K)$–V relationship (Fig. 5 C) is also consistent with the idea that a single type of conformational change (C–O transition) limits I_K relaxation at all voltages.

Scheme IX describes only the response of mSlo channels to voltage and contains no Ca^{2+}-bound states; however, it clearly resembles Scheme I, used earlier to describe the interaction of Ca^{2+} with mSlo channels. Indeed these two models are strictly analogous. Like Scheme I (Cox et al., 1997a), Scheme IX assumes that channels undergo a central rate-limiting conformational change from closed to open, and this transition is allosterically regulated. In Scheme I, interaction of Ca^{2+} with binding sites on each of the four subunits enhances channel opening. In Scheme IX, voltage-dependent conformational changes in each subunit influence channel opening.

An important prediction of Scheme IX is that the limiting behavior of $\tau(I_K)$ should reflect the voltage dependence of C–O transitions. According to the model, horizontal transitions equilibrate rapidly and open channels tend to occupy the left-most state (O_0) at negative voltages such that the time constant of I_K deactivation is determined by the rate constant (γ_0) associated with the O_0 to C_0 transition [$\tau(I_K) = 1/\gamma_0$]. The $\tau(I_K)$–V relationship measured at limiting negative voltages therefore determines the value of γ_0 used in the model and implies that channel closing is weakly voltage dependent ($z_{\gamma 0} = 0.138 \pm 0.003\ e$, $n = 11$). For simplicity, we also assume for Scheme IX that all O to C transitions have the same voltage dependence.

The forward transitions from C to O also appear to be weakly voltage dependent. The rate constant from C_4 to O_4 can be determined by measuring the $\tau(I_K)$–V relationship at limiting positive voltages, where $\tau(I_K) = 1/\delta_4$. Simulations of Scheme IX suggest that this limiting behavior will be observed at voltages greater than +300 mV, which cannot be attained under our experimental conditions. Nonetheless, the voltage dependence of $\tau(I_K)$–V measured from +180 to +280 mV ($z = 0.29 \pm 0.02\ e$) places an upper limit on the charge associated with channel opening (see discussion). We assign a charge $z_\delta = 0.26\ e$ to the forward C–O transitions in the model, giving a total charge of $z_L = 0.40\ e$ for the C–O equilibrium ($z_L = z_\delta + z_\gamma$). This value of z_δ provided reasonable fits to the $\tau(I_K)$–V relationships (Fig. 5), and the resultant value of z_L is also consistent with the voltage dependence of steady state open probability discussed later.

If the C–O transitions in Scheme IX are weakly voltage dependent, then the horizontal transitions involving subunit activation must account for the bulk of the channel's voltage sensitivity. To account for the Δt–V relationship, the Cole-Moore effect, and the voltage dependence of P_o, we have assigned a charge $z_J = 0.55\ e$ and half activation voltage $V_h(J) = +145$ mV to the equilibrium constant for subunit activation:

$$J = e^{(V - V_h)\frac{ez_J}{kT}}.$$

Thus, a total charge of $4z_J = 2.2\ e$ should be associated with the horizontal transitions, and $z_L = 0.4\ e$, or 15% of the estimated total charge ($z_T = z_L + 4z_J = 2.6\ e$), is associated with channel opening.

From a mechanistic standpoint, the assignment of most of the charge to the horizontal transitions in Scheme IX implies that subunit activation involves movement of the channel's intrinsic voltage sensor. Thus Scheme IX not only divides mSlo activation into fast and slow transitions, but also separates voltage-sensor movement from channel opening. In other words, the model suggests that voltage-sensor activation and channel opening represent distinct conformational events that are allosterically coupled.

The Voltage Dependence of Steady State Activation

The conductance–voltage (G_K–V) relationship was measured in 0 Ca^{2+} (at 20°C) using both macroscopic and single channel currents to examine steady state activation over a wide range of voltage and open probability (Fig. 6). Fig. 6 A shows a family of macroscopic I_K evoked in response to 20-ms pulses to different voltages. Steady state conductance (G_K) was determined from tail current amplitudes, normalized to maximal conductance (G_{max}), and plotted against voltage (Fig. 6, B and C). Data from many individual experiments

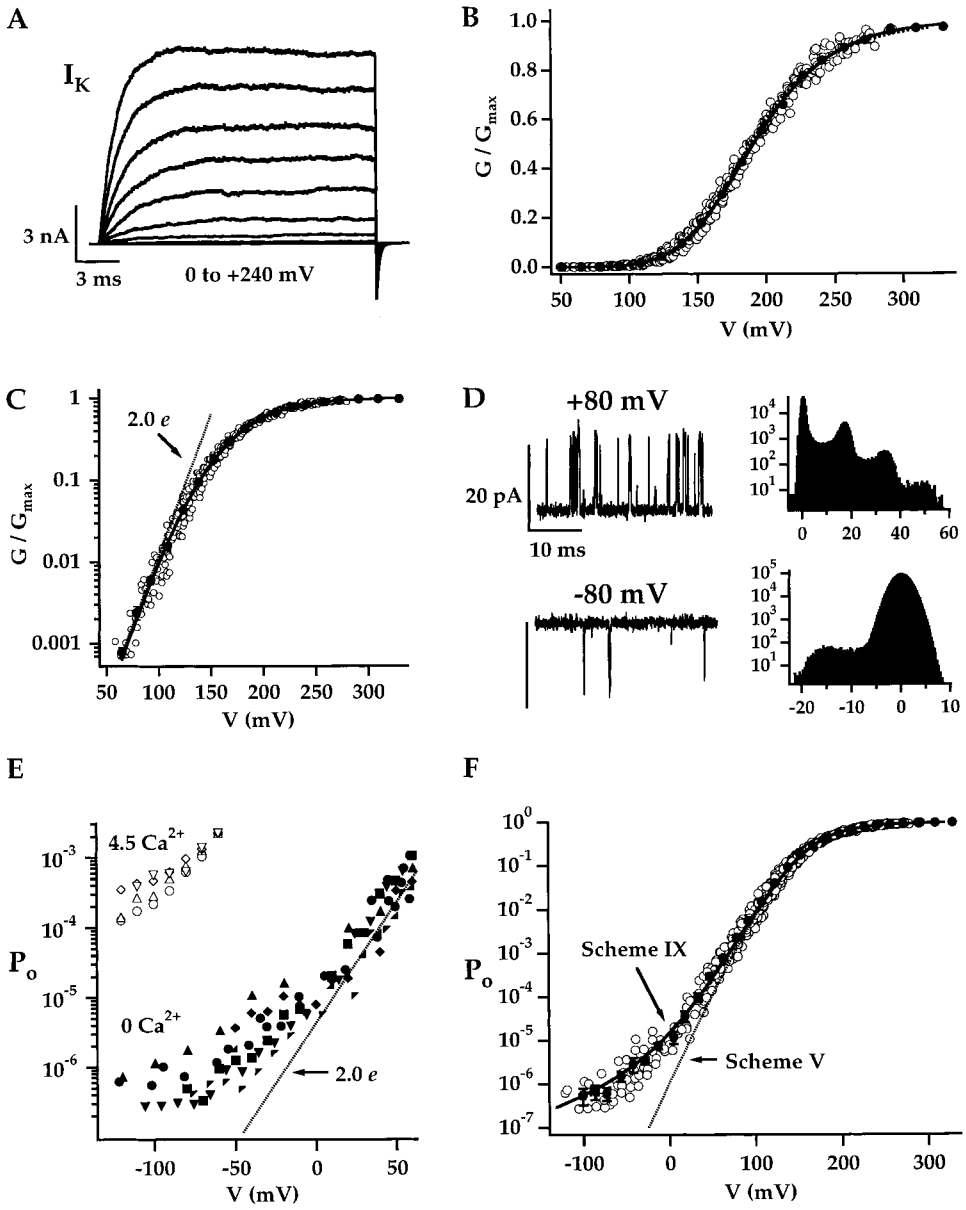

Figure 6. Steady state activation. (A) A family of I_K evoked in response to 20-ms depolarizations (+80 to +280 in 20-mV steps, holding potential = −80, 20°C). $G_K(V)$ was determined by measuring the tail current amplitude at −80 mV immediately after each pulse. (B) The G_K–V relationships from 23 experiments (○) were normalized by G_{Kmax} and shifted along the voltage axis to align half-activation voltages (see methods). The average G–V (●) represents the mean ± SEM of the normalized-shifted data determined over 15-mV intervals. A Boltzmann function raised to a power of 3.2 (z = 0.69 e, solid line) represents the best fit to the individual data, excluding experiments where $V_{max} < 240$ mV. G_{Kmax} could not be directly determined for the excluded experiments; therefore, these data were normalized based on the Boltzmann$^{3.2}$ fit. Dashed lines indicate predictions of Scheme V [$\epsilon = \delta/\gamma$, $\epsilon(0) = 0.367$, $z_\epsilon = 0.295$ e, $z_J = 0.55$ e, $V_h(J) = 145$] and Scheme IX [$L(0) = 2\ e^{-6}$, $z_L = 0.4$ e, $z_J = 0.55$ e, $V_h(J) = 145$, $D = 17$]. (C) The data are replotted on a semi-log scale together with the Boltzmann$^{3.2}$ fit (solid line). The maximum voltage dependence of G–V is indicated by a dashed line (z = 2.0 e). (D) Single channel currents were recorded at the indicated voltages and filtered at 20 kHz. The corresponding all-points histograms are plotted on a semi-log scale (points versus picoamperes). (E) Normalized open probability (P_o/P_{omax}, see text) determined from single channel currents is plotted versus voltage for several experiments in 0 Ca^{2+} (filled symbols) or 4.5 μM Ca^{2+} (open symbols). The dashed line indicates the maximum voltage dependence of the macroscopic G–V from C. (F) The normalized P_o–V relationship from −120 to +300 mV combines the macroscopic and single channel data. Filled symbols indicate averages (mean ± SEM, 15-mV bin width), while open symbols represent data from individual experiments. Predictions of Schemes V (dashed line) and IX (solid line) are the same as in B.

are plotted (○). To compensate for patch-to-patch variation in half-activation voltage, individual plots were shifted along the voltage axis to align them with the mean V_h (190 ± 2.3 mV; SEM, n = 20) (see methods). These shifted data were then combined in 15-mV bins to determine the average G–V (Fig. 6, B and C, ●).

The predictions of sequential Scheme V and the allosteric Scheme IX are superimposed on the data in Fig. 6 B (dashed lines) and are essentially indistinguishable from each other over this voltage range. The G–V can also be well fit by a Boltzmann function that is raised to a power of 3.2 (Fig. 6, B and C, solid line) (Cui et al., 1997). Many sequential models like Scheme V predict a G–V relationship that can be approximated by a Boltzmann function raised to power >1 (Wyman and Gill, 1990; Zagotta et al., 1994b). Such Boltzmann-like functions achieve a maximal limiting voltage dependence at negative voltages. The semi-log plot in Fig. 6 C demonstrates that the data are consistent with a such a relationship over a large range of open probability, and appear to achieve a limiting logarithmic slope of e-fold per 12.6 mV (z = 2 e) (Fig. 6 C, dashed line).

However, while this slope does indicate the maximum voltage dependence of the mSlo G–V, it does not represent the limiting voltage dependence. Measurements of channel activity at more negative voltages (Fig. 6 D) reveal a marked decrease in the voltage dependence of steady state activation (Fig. 6 E), which deviates from a Boltzmann-like G–V relationship (Fig. 6 F) and provides evidence for the presence of multiple open states.

The data in Fig. 6 D were recorded at +80 and −80 mV from a macropatch containing several hundred mSlo channels. At these voltages, where P_o is small ($<10^{-3}$), single channel openings are observed. All-point amplitude histograms like those in Fig. 6 D were constructed by recording such events for 5–45 s and were used to evaluate total open probability at each voltage ($V \leq +80$ mV) (see methods). These data were then normalized based on macroscopic currents recorded in the same patch to determine normalized open probability (P_o/P_{omax}), which is plotted against voltage in Fig. 6 E.

The normalized P_o–V relationships in Fig. 6 E were obtained from several experiments in 0 Ca^{2+} or 4.5 μM Ca^{2+}. P_o/P_{omax} at +80 mV in 0 Ca^{2+} are comparable with those measured from macroscopic currents at the same voltage (Fig. 6 C). Similarly, the voltage dependence of P_o from +20 to +80 mV is comparable with the maximal slope of the macroscopic G–V, indicated by a dashed line in Fig. 6 E. However, a decrease in the slope of the P_o–V relationship is observed at more negative voltages both in the presence and absence of Ca^{2+}. That is, P_o at negative voltages is greater than predicted from the Boltzmann-like fit to the macroscopic G–V. This deviation cannot be due to a failure to detect brief openings, since missed events should be more prominent at negative voltages and lead to an underestimate of P_o. Furthermore, the shape of the normalized P_o–V relationship is similar in the presence or absence of Ca^{2+} despite the fact that Ca^{2+} increases the mean open time (Magleby and Pallotta, 1983b).

The normalized P_o–V relationships obtained from many experiments in 0 Ca^{2+} are plotted on a semi-log scale in Fig. 6 F for voltages from −120 to +300 mV. Filled symbols indicate averages (mean ± SEM, 15-mV bin width) while open symbols represent data from individual experiments. The data from single channel activity ($P_o/P_{omax} < 10^{-3}$) are continuous with the macroscopic data and are weakly voltage dependent at negative voltages where $P_o/P_{omax} = 10^{-5}$–10^{-6}. The prediction of sequential Scheme V is superimposed on the plot (dashed line), the data deviates from this Boltzmann-like relationship for $P_o/P_{omax} < 10^{-4}$. The allosteric model, Scheme IX provides an excellent fit (Fig. 6 F, solid line) over the entire voltage range using the same parameters that describe the $\tau(I_K)$–V relationship in Fig. 5.

The decrease in voltage dependence of steady state activation observed at low P_o could be caused by a small subpopulation of malformed mSlo channels or endogenous channels that fail to close in a normal voltage-dependent manner. However, several lines of evidence argue that the weak voltage dependence of P_o represents the behavior of normal mSlo channels. First, the normalized P_o–V relationships recorded from different experiments are similar (Fig. 6 E) and are therefore unlikely to represent a variable mixture of channel types. Second, the large amplitude of single channel events measured at negative voltages (Fig. 6 D) clearly identify them as mSlo channel currents. Third, P_o is Ca^{2+} sensitive even at potentials where the voltage dependence of P_o is weak (Fig. 6 E). Fourth, the relative probability of observing multichannel openings was well described by a Poisson distribution (data not shown), consistent with the presence of a large uniform population of channels with low P_o, rather than a small subpopulation of malformed channels with high P_o. Finally, although the number of events collected were insufficient to analyze the single channel kinetics in detail, open times observed at −80 mV in 0 Ca^{2+} were very brief (95% were <160 μs, measured with a 50% amplitude criterion), consistent with the observation that macroscopic I_K deactivation is very fast at the same voltage [mean $\tau(I_K)$ = 172 μs at 20°C].

The complex voltage dependence of steady state activation provides support for the conclusions that mSlo voltage gating involves multiple open states and that the C–O transitions are weakly voltage dependent. The limiting voltage dependence of mSlo indicates that a weakly voltage-dependent pathway exists between the resting closed state and an open state even though channel opening at more positive voltages proceeds through one or more voltage-dependent routes. Thus the "limiting slope" of the G–V relationship cannot be used as an estimate of total gating charge for BK channels. This behavior can be explained by models like Scheme IX, where multiple voltage-dependent pathways exist between closed and open states. According to Scheme IX:

$$P_o = \frac{1}{1 + \frac{(1+J)^4}{L(1+DJ)^4}}. \quad (15)$$

At negative voltages, where J is small ($J << 1/D$), this reduces to

$$P_o = \frac{L}{1+L}, \quad (16)$$

if P_o is also small ($L << 1$):

$$P_o = L. \quad (17)$$

Thus, at negative voltages, P_o is determined by the C_0–O_0 equilibrium constant (L). That P_o is weakly voltage dependent is consistent with the notion that C–O transitions are weakly voltage dependent. The fit of Scheme IX to the average data in Fig. 6 F suggests that this limiting behavior of P_o was obtained, and the value of L used in the model ($2*10^{-6}$) is constrained by P_o at negative voltages. However, the limiting voltage dependence of P_o was not measured over a large enough voltage range to directly determine the voltage dependence of L. Therefore z_L was adjusted to provide a reasonable fit to the overall shape of the P_o–V and $\tau(I_K)$–V relationships, as well as the limiting behavior of P_o.

Reproducing "Sequential" Behavior with the Allosteric Gating Scheme

At negative voltages, both the $\tau(I_K)$–V and P_o–V relations are weakly voltage dependent, consistent with the hypothesis that mSlo channels can open and close in a manner that does not involve voltage-sensor movement. We also have described features of mSlo behavior that can be described by a more conventional sequential gating scheme (Scheme V) (e.g., the kinetics and voltage dependence of the delay in I_K activation) and the ability of the macroscopic G–V to be approximated by a Boltzmann function raised to a power greater than one over a large range of P_o. The allosteric model (Scheme IX) also can account for these latter results.

The P_o–V relationship predicted by Scheme IX (Fig. 6 F, Scheme IIb) is almost indistinguishable from that predicted by Scheme V for $P_o > 10^{-3}$. To reproduce this behavior, the allosteric factor (D) in Scheme IX must be large. If D is large, channel opening at positive voltages most likely will occur only after all four voltage sensors have been activated, and the allosteric model then behaves much like a sequential scheme. The value of D (17) used in the model was also constrained by the overall shape of the P_o–V relationship. At very negative voltages, P_o is determined by the C_o–O_o equilibrium constant L; at positive voltages, the C_4–O_4 equilibrium constant (LD^4) becomes more important. Thus, the value of D is critical in determining the relative magnitude of P_o at negative and positive voltages. The half-activation voltage of the G–V [$V_h(P_o)$] also depends upon D, as well as the equilibrium constants L and J. L is fixed by the limiting value of P_o at negative voltages, J is constrained by the voltage dependence of the delay in I_K (see below), and there is little freedom to adjust D without producing unacceptable changes in $V_h(P_o)$.

Figs. 7 and 8 show that Scheme IX can fit the kinetics of I_K activation, using the same parameters that reproduce the $\tau(I_K)$–V and P_o–V relationships. These fits were critical in constraining the model parameters associated with the horizontal transitions, corresponding to voltage-sensor activation.

The results presented in Figs. 1–3 show that mSlo I_K activates with a brief delay and that these kinetics can be approximated by a sequential model (Scheme V) that contains fast voltage-dependent transitions followed by a rate-limiting opening step. However the time course of I'_K was not precisely reproduced by the

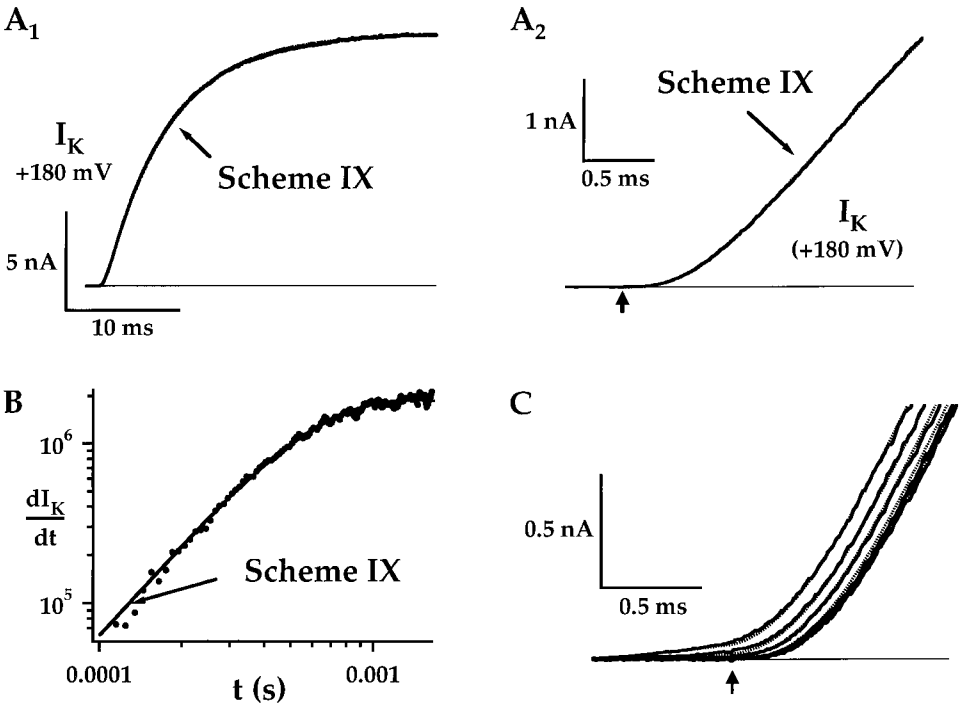

Figure 7. Allosteric model: I_K kinetics. Scheme IX was used to fit the time course of mSlo I_K (solid lines; Table I: Patch 2, $\Delta V_h = -11.3$ mV). (A_1 and A_2) I_K evoked at +180 mV at 7°C (from Fig. 2 A). (B) $d(I_K)/dt$ is plotted on a log–log scale (from Fig. 2 B_2). (C) The Cole-Moore shift (from Fig. 3 A).

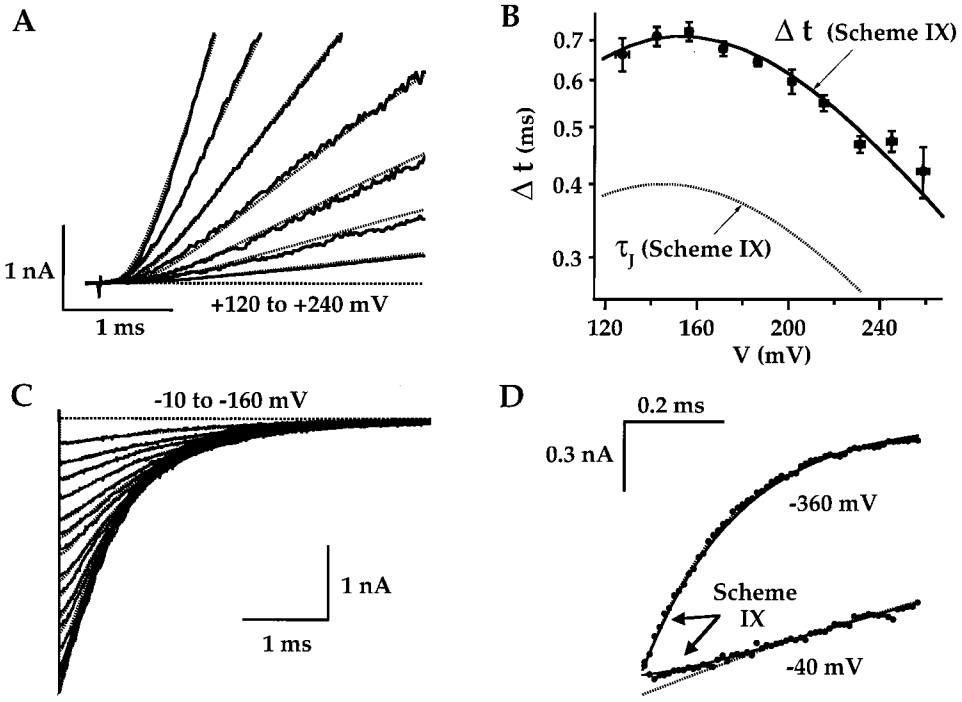

Figure 8. Allosteric model: voltage dependence of I_K kinetics. (A) The initial time course of I_K activation at different voltages (from Fig. 3 B, 5°C) are fit by Scheme IX (Table I: Patch 1, ΔV_h = +5.6 mV). (B) The average Δt–V relationship (from Fig. 3 D) is compared with the prediction of Scheme IX for Δt (solid line) and the time constant of voltage-sensor movement $\tau_J = 1/(\alpha + \beta)$ (dashed line). (Table I: average 5°C). (C) Scheme IX (dashed lines; Table I: Patch 1, ΔV_h = +5.6 mV) predicts a delay in tail currents measured from 0 to −160 mV (from Fig. 4 C). (D) Tail currents and Scheme IX predictions (solid line) at −40 and −360 mV show initial deviation from an exponential fit (dashed lines, from Fig. 4, C and D) at −40 mV, but not at −360 mV. Thus, a tail current delay is observed, but not at very negative voltages.

sequential scheme unless voltage sensors were assumed to interact in a cooperative manner (Scheme VI). The allosteric model can account for these kinetics while assuming voltage sensors act independently. Fig. 7 shows that Scheme IX reproduces the time course and delay in I_K activation (Fig. 7, A_1 and A_2) as well as I'_K (Fig. 7 B) at +180 mV, and the Cole-Moore shift (Fig. 7 C).

In Scheme IX, the delay duration (Δt) is influenced by the time constant associated with voltage-sensor activation while the channel is closed [$\tau_J = 1/(\alpha + \beta)$] and therefore constrains the rate constants associated with C–C transitions. The equilibrium constant J and charge z_J associated with voltage-sensor activation are mainly constrained by the Δt–V and P_o–V relationships. Fig. 8 A shows that the allosteric scheme reproduces the initial time course of I_K activation, and therefore the delay, at different voltages. Fig. 8 B compares the average Δt–V data to the predicted Δt (solid line) and τ_J (dashed line). Scheme IX predicts that the Δt–V and τ_J–V relationships will be similar in shape but, in contrast to Scheme V, their maxima will not be at the same voltage [$V_{max}(\Delta t)$ = 153 mV, $V_{max}(\tau_J)$ = 145 mV]. This small difference, representing a voltage-dependent change in the relationship between Δt and τ_J, reflects the ability of channels to open before all four voltage sensors are activated. The Δt–V relationship was measured mainly at voltages more positive than $V_{max}(\Delta t)$, and therefore constrains the charge associated with voltage-sensor activation (z_α) more tightly than that associated with deactivation (z_β). For simplicity, Δt–V was fit with the assumption that τ_J is symmetrically voltage dependent, yielding $z_\alpha = -z_\beta = 0.275\ e$. Although the Δt–V data do not require symmetry, values of z_α and z_β close to these estimates are necessary to assign a reasonable total charge [$z_J = (z_\alpha + z_\beta) = 0.55\ e$] to voltage-sensor activation. z_J is constrained by the fit to the P_o–V relationship (Fig. 6 F) and is consistent with the $\tau(I_K)$–V relationship (Fig. 5, B and C) and Cole-Moore shift (Fig. 7 C). The accompanying paper shows that this estimate of z_J is also consistent with gating current measurements (Horrigan and Aldrich, 1999).

Delay in I_K Deactivation

One feature of Scheme IX that distinguishes it from models with a single open state is that it predicts a delay in I_K deactivation because channels can pass through several open states before closing. Tail currents in Fig. 4 C exhibit a slight delay, which is evident as a deviation from an exponential fit during the first 200 μs after a voltage pulse. Even at 5°C, this delay is brief and could be influenced by filter properties or series-resistance error. However, tail currents at more negative voltages in the same patch (Fig. 4 D) did not show such a deviation from exponential decay, suggesting that the tail current delay is not an artifact. The allosteric model reproduces these tail current kinetics, as shown in Fig. 8 C. Fig. 8 D compares tail currents and simulations at −40 and −360 mV. The data and prediction of Scheme IX (solid lines) deviate from an exponential time course (dashed lines) at −40 but not −360 mV. The delay disappears at very negative voltages because the time con-

stant associated with open-state transitions, representing voltage-sensor deactivation, decreases at negative voltages. It should be noted that, according to the allosteric model, the equilibrium constants for open-state transitions differ from those for closed state transitions by a factor *D*. Thus, open- and closed-state transitions are expected to be characterized by different time constants. We expressed this difference as an increase in the forward O–O rate constants by $\sqrt{D}$ and a decrease in the backward rates by the same factor relative to the corresponding C–C transitions.

discussion

We have studied mSlo channel currents at very low $[Ca^{2+}]_i$ to elucidate the mechanism of voltage-dependent gating. This procedure limits the number of accessible conformations to those without Ca^{2+} bound. To a first approximation, the voltage response of mSlo channels appears simpler than that of many voltage-sensitive channels and can reasonably be described by a two-state gating scheme (Cui et al., 1997). For example, the time course of macroscopic I_K activation is well fit by an exponential function after a brief delay, and the time constant of I_K relaxation is much slower than the delay. At voltages where steady state P_o is significant ($>10^{-3}$), the kinetics of both activation and deactivation exhibit an exponential voltage dependence (Fig. 5 A) consistent with the presence of voltage-dependent forward and backward transitions between a closed and an open state. Finally, when estimates of equivalent charge associated with these transitions are summed, they are similar to that obtained by fitting the steady state G_K–V relationship with a Boltzmann function (Cox et al., 1997a).

These characteristics of mSlo gating appear simple and self-consistent, but closer examination of I_K kinetics and voltage dependence over a wider range of conditions reveals deviations from two-state behavior that imply a surprisingly complex underlying gating mechanism. An important conclusion of this study is that mSlo channel opening and voltage-sensor activation reflect distinct conformational events that occur on different time scales but are allosterically coupled. Based on the assumption that the channel has a voltage sensor in each of four identical subunits, this mechanism results in a 10-state gating scheme with five open and five closed states arranged in parallel. In this allosteric model, transitions among closed (C–C) or open (O–O) states are governed by rapid voltage sensor movements, while closed–open (C–O) transitions are weakly voltage dependent and rate limiting. Because voltage-sensor activation is assumed to be much faster than channel opening, this scheme predicts exponential relaxation kinetics and other "simple" behaviors that can be approximated by a two-state model or a sequential gating scheme. However, these properties change with voltage in a manner that reflects the complexity of the underlying mechanism. In particular, the kinetic and steady state properties of I_K activation become weakly voltage dependent at negative voltages, suggesting that channel opening can occur in the absence of voltage-sensor activation.

The allosteric model of mSlo voltage gating has implications for understanding BK channel activation and voltage-dependent channel gating in general. First, the model establishes a framework for evaluating the effects of mutation on voltage-dependent BK channel gating. Second, the scheme forms a basis for understanding the effects of Ca^{2+} on BK channel gating. The demonstrated complexity of mSlo voltage gating in the absence of Ca^{2+} greatly increases the minimum complexity of models that include Ca^{2+}-bound states. The voltage-gating mechanism also raises the fundamental question whether Ca^{2+} acts by modulating voltage-sensor movement, channel opening, or some combination of both of these processes. Finally, the allosteric scheme may apply to other voltage-dependent channels. The following discussion considers these implications of the model in detail.

Allosteric Voltage Gating and the Effect of S4 Mutation

The allosteric gating scheme has implications for interpreting BK channel structure–function studies because some apparently simple features of macroscopic I_K kinetics and voltage dependence may be related in a complicated manner to elementary molecular events such as voltage-sensor movement and channel opening. This is illustrated by the example in Fig. 9.

Neutralization of a charged residue in the S4 segment of mSlo (R207Q) produces a marked decrease in the steepness of the G–V relationship and a shift of almost −100 mV in the half-activation voltage (Fig. 9 A) (Diaz et al., 1998; Cui, J., and R.W. Aldrich, manuscript in preparation). The S4 segment is thought to form part of the voltage sensor in voltage-gated channels and a reasonable hypothesis is that the mutation reduces the charge associated with voltage-sensor movement, thereby reducing the voltage dependence of channel activation. If mSlo channel voltage gating could be described by a two-state model, a decrease in gating charge would be required to account for a change in the steepness of the G–V. However, the allosteric model suggests a different explanation.

The wild-type (WT) G–V in Fig. 9 A was fitted by allosteric Scheme IX (solid line) using the same parameters as in Fig. 6 F. The R207Q G–V was then fit (solid line) by changing the half-activation voltage for the voltage sensor $[V_h(J)]$ from +145 to −100 mV and leaving all other parameters the same as for the WT. That is, the effect of the S4 mutation can be accounted for

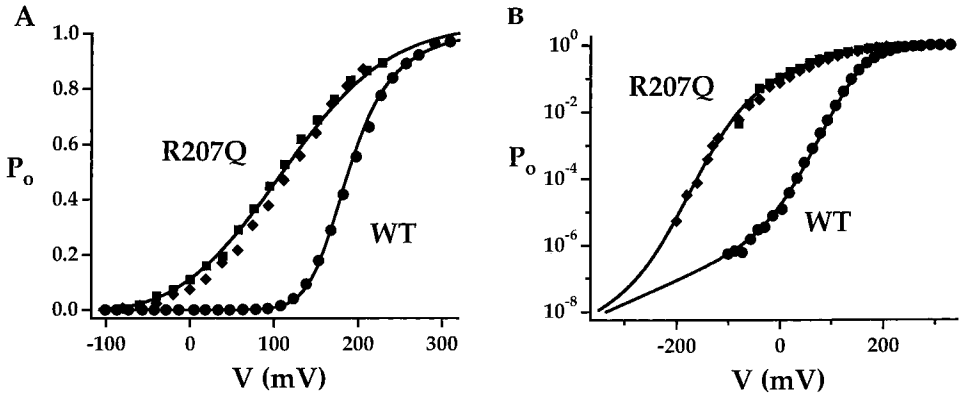

Figure 9. Effect of S4 mutation. G_K–V relationships for mSlo WT and S4 mutant R207Q in 0 Ca^{2+} were obtained using both macroscopic and single channel currents as in Fig. 6 and are plotted on linear (A) and semi-log (B) scales. Scheme IX was used to fit both relationships (solid lines). Parameters are the same as in Fig. 6 [$L(0) = 2\ e^{-6}$, $z_L = 0.4\ e$, $z_J = 0.55\ e$, $D = 17$], except $V_h(J) = -100$ mV for R207Q, while $V_h(J) = 145$ mV for WT.

by increasing the equilibrium constant J 207-fold ($\Delta\Delta G = 5.33\ kT$) without changing the voltage sensor charge (z_J), the allosteric factor (D), the C–O equilibrium constant (L), or the charge associated with channel opening (z_L).

According to the allosteric model, the shape of the G–V for R207Q mainly reflects the charge associated with the C_4–O_4 transition (z_L) because the voltage sensors are largely activated at voltages where P_o is small. Thus the WT G–V is steeper because voltage-sensor activation and channel opening occur over the same voltage range. To test this conclusion, R207Q activation was examined at low P_o (Fig. 9 B). The voltage dependence of P_o for the mutant increases at negative voltages to a maximum slope like that exhibited by the WT (Diaz et al., 1998). This behavior is reproduced by Scheme IX (Fig. 9, solid lines), reflecting the ability of mutant voltage sensors to become deactivated at negative voltages, and consistent with the idea that the total gating charge for the two channels are similar. Gating charge measurements for WT and mutant channels in the companion article (Horrigan and Aldrich, 1999) support this conclusion.

Allosteric Voltage Gating and the Voltage Dependence of $\tau(I_K)$

The voltage dependence of I_K relaxation kinetics is another feature of mSlo gating that illustrates a complex relationship between molecular events and macroscopic behavior. As shown in Fig. 4 C and previously reported by Cox et al. (1997a), the time constant of I_K relaxation exhibits a bell-shaped voltage dependence over a 250-mV voltage range centered near the half-activation voltage for mSlo. The two regions of exponential voltage dependence might reasonably be interpreted as representing the voltage dependencies of rate limiting forward and backward transitions between single closed and open states. However, the allosteric scheme suggests that this apparently simple voltage dependence is an emergent feature of all transitions in the model and cannot be attributed to properties of individual rate constants.

According to Scheme IX, the horizontal C–C and O–O transitions will be so fast that they do not affect $\tau(I_K)$. This point was confirmed in Fig. 10 A by showing that the values of $\tau(I_K)$ measured from I_K simulations (symbols) can be reproduced by an analytical approximation of the $\tau(I_K)$–V relationship (solid line) that assumes horizontal transitions are equilibrated:

$$\tau(I_K) = \left[\sum_i (\delta_i pC_i + \gamma_i pO_i)\right]^{-1}, \qquad (18)$$

where δ_i and γ_i are rate constants for the C_i–O_i transitions and pC_i and pO_i are conditional occupancies of the open and closed states [$pC_i = p(C_i|C)$ and $pO_i = p(O_i|O)$].

The shape of the $\tau(I_K)$–V relationship can to some extent be explained by comparing it to the time constants of the individual C–O transitions in the model [$\tau_i = (\delta_i + \gamma_i)^{-1}$] (Fig. 10 A, τ_0–τ_4, dashed lines). At limiting negative voltages, $\tau(I_K)$ is determined by the time constant of the C_0–O_0 transition (τ_0) and at positive voltages by the C_4–O_4 transition (τ_4). At intermediate voltages, $\tau(I_K)$ represents a weighted sum of the rate constants for all C–O transitions (Eq. 18), where the relative weighting depends on the equilibrium distributions of different closed and open states [$pC_i(V)$ and $pO_i(V)$]. The time constants of individual C–O transitions (τ_i) provide a rough indication of the range spanned by $\tau(I_K)$ at intermediate voltages. However, $\tau(I_K)$ measured from +30 to +240 mV in Fig. 4 C reflects the voltage dependence of the horizontal equilibria in the model as well as the kinetics of the different C–O transitions, and cannot be attributed to a particular rate-limiting step. Thus, the exponential voltage dependence of $\tau(I_K)$ at intermediate voltages is coincidental and does not represent the voltage dependence of any one rate constant [although $\tau(I_K)$ can not be attributed to single rate constants, the rate-limiting transition always represent the C–O conformational change].

The simulation in Fig. 10 A predicts that $\tau(I_K)$ will achieve a limiting voltage dependence, representing the

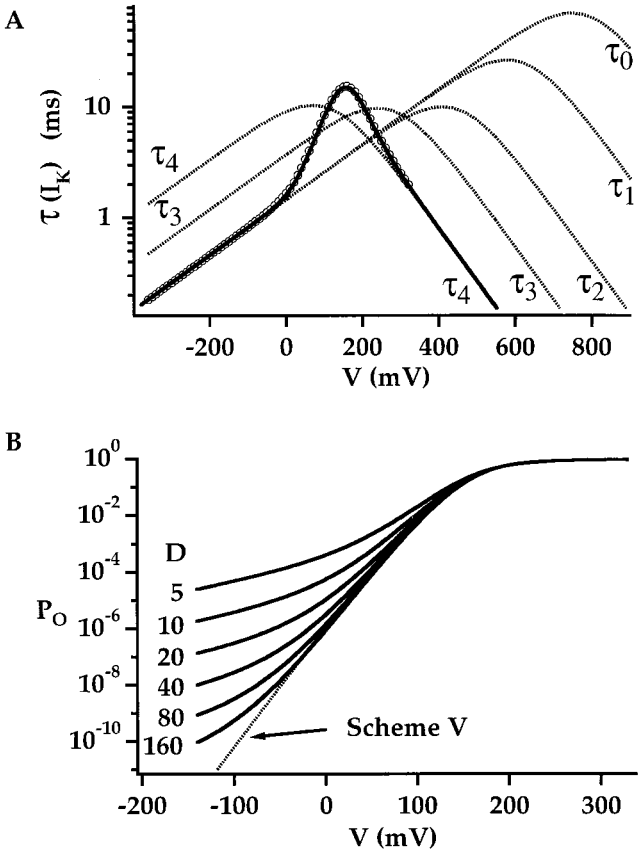

Figure 10. Properties of the allosteric voltage-gating scheme. (A) The $\tau(I_K)$–V relationship determined by simulating Scheme IX (●; Table I: average 5°C) can be reproduced by an analytical approximation (solid line) that assumes horizontal transitions are equilibrated. The voltage dependence of time constants for individual C–O transitions are also plotted ($\tau_i = [\delta_i + \gamma_i)^{-1}$]. (B) P_o–V relationships predicted by Scheme IX (solid lines) are plotted on a semi-log scale as the allosteric factor D is adjusted [with $z_L = 0.4\ e$, $z_J = 0.55\ e$, $V_h(J) = 145$]. The equilibrium constant L was adjusted together with D such that the half-activation voltage remained constant (for D = 5–160: $L = 2.18\ e^{-4}$, $1.57\ e^{-5}$, $1.05\ e^{-6}$, $6.80\ e^{-8}$, $4.33\ e^{-9}$, and $2.72\ e^{-10}$). A dashed line indicates the prediction of sequential Scheme V (from Fig. 6).

charge associated with the C_4–O_4 transition (z_δ), at voltages (>300 mV) that exceed our experimental range. Therefore, we used the exponential voltage dependence of $\tau(I_K)$ between +180 and +280 mV ($z_{(180–280)} = 0.29\ e$) as an upper limit for z_δ. For parameters that describe our data, Scheme IX always predicted $z_{(180–280)} \geq z_\delta$. This is not a general property of the model, however.

The allosteric model requires that the equilibrium constant for C–O transitions increase D-fold for each voltage sensor that is activated. The forward and backward rate constants are not otherwise constrained. $\tau(I_K)$–V relationships in Fig. 5 were fit with the additional assumption that forward rates increase and backward rates decrease monotonically with each voltage sensor activated. A conclusion of this analysis is that voltage-sensor activation affects mainly the forward rate constants. Fits to the 5° or 20°C data in Fig. 5 C required that the forward rates increase 11,500- or 6,700-fold when all four voltage sensors are activated, whereas the backward rates decrease only 7.3- or 12.5-fold, respectively. Indeed, the backward rates for the first three C–O transitions were assumed to be identical such that τ_0, τ_1, and τ_2 are identical at negative voltages as shown in Fig. 10 A. This result suggests that voltage-sensor activation may destabilize the closed conformation with little effect on the free energy of the open conformation or the transition barrier between O and C.

Allosteric Versus Sequential Gating Schemes

An important feature of the mSlo data that is reproduced by the allosteric model is that many kinetic and steady state properties of I_K can be approximated by a sequential gating scheme (Scheme V), except at extreme voltages. This is significant because many voltage-gated channels have been described by sequential models analogous to Scheme V; it is possible that such channels also operate through an allosteric mechanism, but have not been studied under conditions that reveal such a mechanism.

The distinction between allosteric and sequential schemes is important because the models make different predictions concerning the possible molecular events that link voltage-sensor movement to channel opening (discussed below). In addition, the allosteric scheme provides a simple explanation for cooperative interaction of voltage-sensors in voltage-dependent gating. Many channels exhibit behaviors that deviate from the predictions of completely independent schemes such as the Hodgkin–Huxley model (Hodgkin and Huxley, 1952). Such results can be described by gating schemes in which the voltage sensors interact in a cooperative manner such that the activation of one affects the movement of the others (Vandenberg and Bezanilla, 1991; Perozo et al., 1992; Tytgat and Hess, 1992; Zagotta et al., 1994a). We have used such a model (Scheme VI) to fit the delay in mSlo I_K activation. Scheme VI implies that there is direct communication between voltage sensors in different subunits. The allosteric model (Scheme IX) can account for the delay kinetics, as well as other features that are not reproduced by Scheme VI, using the simpler assumption that voltage sensors act independently while the channel is either closed or open. Cooperativity is embodied in the allosteric transition between these two conformations, a mechanism of subunit–subunit communication that is known to exist in many proteins (Perutz, 1989).

Given the ability of allosteric and sequential models to act similarly, it is important to define the conditions that allow them to be distinguished. The ability of the allosteric model to act like a sequential scheme was il-

lustrated by the comparison of P_o–V relationships for Schemes V and IX Fig. 6 F. The two predictions deviate significantly from each other only when P_o is very small ($P_o < 10^{-4}$); the two models cannot be distinguished based on conventional G–V measurements. The allosteric model for mSlo behaves like a sequential scheme because the allosteric factor is large ($D = 17$), such that the equilibrium constant for the C–O transition increases by a factor of 83,000 (D^4) when all voltage sensors are in the activated state. Channel opening is most likely to occur after all voltage sensors have been activated, as in a sequential scheme.

The conditions under which Schemes V and IX converge can be defined by comparing the expression for P_o from Scheme IX (Eq. 15) with that for a version of Scheme V (see Eq. 19), where the C_4-O_4 transition is assigned an equilibrium constant of LD^4, equivalent to the C_4–O_4 transition in Scheme IX.

$$P_o = \frac{1}{1 + \frac{(1+J)^4}{L(DJ)^4}} \tag{19}$$

Eqs. 15 and 19 are equivalent when DJ is large ($>>1$), so we can define a value of J (J_{eq}) such that Schemes IX and V behave equivalently when $J \geq J_{eq}$:

$$J_{eq} \gg 1/D. \tag{20}$$

The value of P_o where these two models converge (P_{eq}) is obtained by substituting J_{eq} into Eq. 19:

$$P_{eq} = \frac{1}{1 + \frac{(1+J_{eq})^4}{LD^4(J_{eq})^4}}. \tag{21}$$

For constant LD^4, P_{eq} will decrease when J_{eq} decreases (when D increases). For large Ds, it is necessary to measure small P_o to observe a divergence between the predictions of the allosteric and sequential models. This is illustrated in Fig. 10 B, which compares P_o–V relationships predicted by Scheme IX for different values of D (5–160). As D is increased, the predictions of Scheme IX (solid lines) become increasingly difficult to distinguish from that of Scheme V (Fig. 10 B, dashed line).

Detection of Allosteric Voltage-gating Behavior

It is quite possible that a channel that activates through an allosteric voltage-gating mechanism mistakenly could be described by a sequential model if the allosteric factor (D) is large. The mSlo data was fit with $D = 17$, indicating that each activated voltage sensor changes the free energy difference between closed and open conformations by $\Delta\Delta G_{co} = \ln(D) = 2.83\ kT$. If this interaction energy were increased by only 55% such that $D = 80$, measurements at $P_o < 10^{-8}$ would be required before deviations from a sequential scheme could be detected (Fig. 10 B).

Additional factors could serve to prevent identification of an allosteric mechanism. Deviations from sequential gating behavior were only clearly demonstrated for mSlo by studying ionic currents at extreme negative voltages and very low P_o, where the voltage sensors are presumed to be in a resting state such that the kinetic and steady state properties of I_K are determined by the C_0–O_0 transition. In the case of mSlo, the equilibrium constant for this transition (L) is large enough that P_o can be measured when voltage sensors are not activated. Similarly, the kinetics and weak voltage dependence of the O_0–C_0 transition allow us to resolve tail current kinetics at voltages as low as −500 mV. In channels where the O_0–C_0 transition is faster or its equilibrium constant smaller than that of mSlo, measurement of ionic current properties may be impractical under conditions that distinguish allosteric and sequential schemes.

The voltages at which P_o can be measured may also limit the identification of an allosteric mechanism. This point is illustrated by the behavior of the mSlo R207Q mutant (Fig. 9). In contrast to the wild type, the slope of the P_o–V relationship for R207Q does not appear to decrease at negative voltages (Fig. 9 B), even though measurements were made down to −180 mV where P_o is very small (10^{-5}). However, both WT and R207Q P_o–V relationships are well fit by the allosteric model using identical values of D, L, z_L, and z_J, and different values of $V_h(J)$ (Fig. 9 B, solid lines). These fits imply that P_o is more steeply voltage dependent for the mutant because the voltage sensors are significantly activated even at −180 mV [$V_h(J) = -100$ mV]. The model predicts that R207Q will achieve the same limiting slope as the WT, but only at voltages more negative than −200 mV (Fig. 9 B). Thus, the identification of a weakly voltage-dependent limiting slope may be impossible if P_o cannot be measured at voltages sufficiently negative to force the voltage sensors into the resting state.

Previous Evidence for Allosteric Voltage Gating

Allosteric models analogous to Scheme IX have been proposed to describe the voltage-dependent activation of several channels, including L-type Ca^{2+} channels (Marks and Jones, 1992), *Shaker* K^+ channels (McCormack et al., 1994), and SR Ca^{2+}-release channels (Ríos et al., 1993). These examples are relevant to the above discussion, present some interesting contrasts to mSlo, and illustrate an alternative approach to testing the allosteric model. In all three studies, it was the action of a ligand rather than the properties of gating under control (ligand-free) conditions that provided the most compelling evidence for an allosteric voltage-gating mechanism. In other words, gating properties in the

absence of ligand were consistent with an allosteric model, but were also adequately described by sequential schemes analogous to Scheme V or VI. Measurements were not performed at extreme voltages or low P_o to distinguish these possibilities. And the allosteric model parameters L and D that were used to describe these channels suggest that such measurements would be at least as difficult as they are for mSlo: $L = 7.8 * 10^{-10}$, $D = 225$ (Marks and Jones, 1992); $L = 1.7 * 10^{-5}$, $D = 49$ (McCormack et al., 1994); and $L = 1.3 * 10^{-6}$, $D = 25$ (Ríos et al., 1993). However, upon ligand application, channel gating was altered in complex ways that were most simply explained in the context of an allosteric voltage-gating mechanism.

Marks and Jones (1992) found that application of dihydropyridine agonists to Ca^{2+} channels caused a decreased latency to first opening, an increase in the maximum P_o, and a slowing of I_{Ca} tail currents. In addition, the P_o–V relationship was shifted to more negative voltages and became steeper. These diverse effects cannot be accounted for by a sequential scheme without assuming that ligand binding has complex effects on multiple transitions. In contrast, an allosteric scheme reproduces all the results with the simple assumption that agonist-binding increases the equilibrium constant (L) for the allosteric C–O transition. The decrease in first latency reflects that an increase in L will allow channels to open when fewer than four voltage sensors are activated. Consistent with this prediction, two open dwell-time components were detected in the presence of ligand, providing evidence for multiple open states. And the predictions of the allosteric model concerning first latency are analogous to those concerning the kinetics of the macroscopic delay in the present study.

Ríos et. al. (1993) also concluded that multiple effects of an agonist (perchlorate) on SR Ca^{2+}-release channel conductance and gating currents could be explained simply in terms of an allosteric model where agonist binding enhances the allosteric transition (increasing L). Conversely, McCormack et al. (1994) proposed that inhibitory effects of 4AP on ionic and gating currents in *Shaker* channels can be explained in terms of a decrease in L that favors the closed conformation.

In line with our results for mSlo, the three studies discussed above concluded that the allosteric transition between C and O was weakly voltage dependent or voltage independent. An important difference between these channels and mSlo is that their activation kinetics appear to be limited by voltage-sensor movement rather than channel opening. In the case of the Ca^{2+} channel (Marks and Jones, 1992), C–O transitions are ~100-fold faster than voltage-sensor activation, essentially opposite the relationship observed for mSlo. This difference results in activation kinetics for Ca^{2+} channels and *Shaker* K^+ channels that are more sigmoidal than observed for mSlo (Zagotta et al., 1994b). Related differences in channel behavior are observed at the level of gating current kinetics (Horrigan and Aldrich, 1999). The relative speed of voltage-sensor movement and channel opening for mSlo turn out to be advantageous for dissecting transitions in the allosteric scheme. For example, we are able to assume that the delay in I_K activation mainly reflects voltage-sensor properties because channel opening is slow. Similarly, the I_K relaxation time constant $\tau(I_K)$ was analyzed with the assumption that voltage sensors are equilibrated.

Limiting Slope of the P_o–V Relationship and Multiple Open States

Measurements of the limiting voltage dependence or "limiting slope" of the G–V relationship have been used extensively to estimate the total gating charge associated with activation of many voltage-gated channels (Almers, 1978; Zagotta et al., 1994b; Hirschberg et al., 1995; Noceti et al., 1996; Seoh et al., 1996) including BK channels (Diaz et al., 1998). Almers (1978) showed that if channel gating can be described by a linear sequence of closed states followed by a single open state, then the voltage dependence of P_o will be maximal at limiting negative voltages. Sigg and Bezanilla (1997) generalized this conclusion to any model containing a single open state. For such schemes, the limiting voltage dependence of P_o denotes the total gating charge moved during a transition from the resting closed state occupied at negative voltages (e.g., C_0 in Scheme V) to the open state. In the few previous instances where single channel currents have been used to measure very low values of P_o, the voltage dependence of P_o appeared to achieve a maximum at negative voltages consistent with the presence of a single open state (Hirschberg et al., 1995; Islas and Sigworth, 1996). However our results show that BK channel gating is not consistent with such a model since the voltage dependence of P_o for mSlo decreases at negative voltages.

When the limiting and maximum voltage dependence of P_o are different, as for mSlo, then the channel must have multiple open states and there must be voltage-dependent pathways between the open states (Sigg and Bezanilla, 1997). The allosteric voltage-gating scheme encompasses these general conclusions. A particular feature of this scheme is that the maximum slope of the P_o–V relationship reflects the charge associated with a subset of transitions and therefore underestimates the total gating charge. For example, the maximum slope of the fit in Fig. 6 F represents an equivalent charge of 1.74 *e*, underestimating the total charge (2.6 *e*) by 33%. In addition, the relationship between maximum slope and total charge may change when model parameters L or D are altered, and changes

in maximum slope caused by channel mutations, such as those reported by Diaz et al. (1998), cannot be unequivocally attributed to changes in total gating charge.

Molecular Mechanism of Allosteric Voltage Gating

Experiments in many voltage-gated channels suggest that the S4 transmembrane segment forms at least part of the voltage sensor (Yang and Horn, 1995; Aggarwal and MacKinnon, 1996; Bao et al., 1999; Larsson et al., 1996; Mannuzzu et al., 1996; Seoh et al., 1996; Yang et al., 1996; Yusaf et al., 1996). Residues have also been identified that may form part of an activation gate that controls the flow of ions through the pore (Liu et al., 1997; Holmgren et al., 1998; Perozo et al., 1998). However, little is known about the molecular nature of the interaction between voltage sensors and the activation gates. Sequential models of voltage gating (Schemes III or V) suggest that voltage sensors form part of the activation gate or are directly linked to the gate in such a way that channel opening can only occur when all voltage sensors are in an activated conformation (Fig. 11 A). In contrast, the allosteric voltage-gating model for mSlo implies a less direct interaction between voltage sensor and channel pore, which is more difficult to envisage in terms of a physical model.

Many allosteric proteins have been studied whose molecular structure is known in detail, such as hemoglobin, glycogen phosphorylase, phosphofructokinase, and aspartate transcarbamoylase (reviewed by Perutz, 1989). These studies provide guidelines concerning the molecular nature of allosteric interactions that could prove useful in understanding how voltage-sensor movement and channel opening might interact in mSlo. These examples are multimeric proteins with multiple ligand-binding sites. Cooperative ligand interactions with these proteins are well described by models analogous to the MWC scheme, where the protein can undergo an allosteric conformational change that in turn affects the affinity of ligand binding sites. In all cases, the high and low affinity conformations of these proteins have been determined by x-ray crystallography. Two important conclusions from these studies are that allosteric transitions generally involve a concerted quaternary conformational change, and that the interaction of ligand-binding sites with the allosteric transition is mediated through subunit interfaces. One explanation for these results is that molecular interactions between subunits are weaker than those within subunits. Thus, a change in the tertiary conformation of a subunit due to ligand binding is more likely to alter the relative position and bonds between subunits than it is to perturb the tertiary conformation of an adjacent subunit. Ligand-binding sites in allosteric proteins are linked to subunit interfaces in such a way that a change

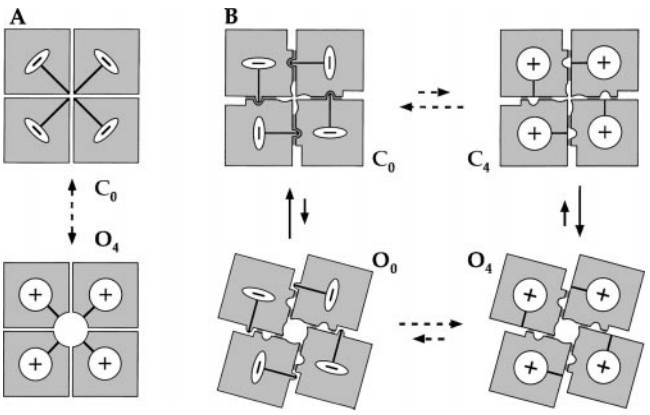

Figure 11. Interaction between voltage sensors and channel gating. Cartoons illustrate two hypothetical mechanisms of coupling between voltage-sensor movement and channel opening. Voltage sensors in each subunit are shown to undergo a transition between resting (−) and activated (+) conformations. For simplicity, only states with all four voltage sensors in the same conformation are shown. The independent transitions of voltage sensors are abbreviated by dashed arrows. (A) A direct coupling mechanism assumes there exists a direct physical link between voltage sensor and a gate that controls the flow of ions through the pore. Such a mechanism does not allow channels to open unless voltage sensors are activated. (B) An allosteric mechanism assumes that channel opening involves a quaternary rearrangement of subunits that alters subunit–subunit interactions (indicated by shaded areas between subunits). Voltage-sensor activation is also assumed to affect subunit–subunit interaction, and is shown here as stabilizing the closed state when voltage sensors are in the (−) conformation.

in quaternary conformation is translated into a change in the structure of the binding site. Quaternary conformational changes often preserve a symmetric arrangement of subunits and are therefore concerted.

By analogy with other allosteric proteins, it is reasonable to propose that mSlo channel opening involves a quaternary conformational change and that voltage sensors affect the interaction between subunits. Structural studies of gap–junction channels and nicotinic Ach-receptor channels by Unwin and co-workers (Unwin and Ennis, 1984; Unwin et al., 1988; Unwin, 1998) support the idea that channel opening involves a quaternary rearrangement of subunits. Experiments examining the accessibility of *Shaker* channels to cysteine-modifying reagents are also suggestive of such conformational changes in voltage-gated channels (Holmgren et al., 1998). Voltage sensors might then affect channel opening if their activation produces a change in the steric or binding interactions between subunits. Fig. 11 B illustrates how such a mechanism might work in the context of the allosteric voltage-gating scheme. In this cartoon, channel opening is depicted as a concerted rotation of four subunits and voltage-sensor activation is shown as a tertiary conformational change within each subunit. For simplicity, only the states with all four voltage sensors in the resting (−) or activated

(+) states are shown, and transitions involving independent voltage-sensor movement are abbreviated by dashed arrows. Shaded areas between subunits represent hypothetical regions of subunit–subunit interaction. Voltage sensors are shown as interacting strongly with adjacent subunits only when they are in the resting conformation and when the channel is closed. Thus, voltage-sensor activation promotes channel opening by selectively destabilizing the closed conformation, as suggested by the kinetic data. Conversely, the equilibrium constant for voltage-sensor activation increases when the channel is open because the resting (−) state is no longer stabilized via interaction with adjacent subunits. Although the details of Fig. 11 B are speculative, they are consistent with our data and suggest a possible molecular mechanism for interaction between voltage sensors and channel opening that may guide future investigation.

The Voltage Dependence of Channel Opening

The idea that mSlo channel opening involves a quaternary conformational change is attractive not only because it is consistent with an allosteric mechanism, but also because it provides a possible explanation for the voltage dependence of channel opening. The allosteric model assumes that channel opening and voltage-sensor activation are distinct events. Yet the data suggest that C–O transitions are voltage dependent and account for ~15% of the total gating charge movement. This result may appear to contradict the assumption that the C–O conformational change does not involve voltage-sensor activation. However, it is likely that channel opening could involve the movement of charged groups in the voltage sensor without requiring that voltage sensors "activate." Quaternary conformational changes in proteins often involve rotations of subunits about an axis perpendicular to the axis of symmetry (Perutz, 1989). In the case of ion channels, such a motion might allow voltage sensors to rotate within the membrane electric field. Thus, channel opening could involve a displacement of voltage-sensor charge without requiring that voltage sensors undergo a tertiary conformational change (from R to A). This mechanism suggests that an alteration in voltage-sensor charge could affect the charge movement associated with both voltage-sensor activation and channel opening. We did not test this prediction, but several investigations of *Shaker* K^+ channels have concluded that 10–17% of the total gating charge (z_T) is associated with channel opening (McCormack et al., 1994; Zagotta et al., 1994a; Smith-Maxwell et al., 1998; Ledwell and Aldrich, 1999) or final cooperative transitions (Schoppa et al., 1992; Sigworth, 1994; Schoppa and Sigworth, 1998b). Thus, the fraction of z_T associated with channel opening is similar for *Shaker* and mSlo even though z_T is approximately fivefold greater for *Shaker* (Horrigan and Aldrich, 1999). This is consistent with *mSlo* and *Shaker* undergoing similar conformational changes, with the difference that the *Shaker* voltage sensor is more highly charged. In addition, mutations to the *Shaker* S4 segment can almost eliminate the voltage dependence of channel gating (Bao et al., 1999), consistent with a reduction of voltage-sensor charge contributing to a decrease in the voltage dependence of the channel opening transition.

Implications for Calcium-dependent Activation

The allosteric voltage-gating scheme has implications for understanding the effects of Ca^{2+} on BK channel function. Many of the effects of Ca^{2+} on mSlo channel activation can be described by a voltage-dependent MWC scheme, which operates under the assumption that Ca^{2+} allosterically modulates voltage-dependent channel activation (Cox et al., 1997a; Cui et al., 1997). This scheme further assumes that channel opening can be described by a single concerted voltage-dependent transition between a closed and open conformation. However, we have shown here that the voltage-dependent activation pathway is more complicated and can be separated into voltage-sensor movement and channel-opening steps. This description of voltage gating raises a question concerning the mechanism of Ca^{2+}-dependent action: Does Ca^{2+} alter voltage-sensor movement or channel opening, or some combination of both? This question will be addressed in a subsequent article (Horrigan, F.T., and R.W. Aldrich, manuscript in preparation).

Regardless of the mechanism of Ca^{2+} sensitivity, the complexity of the allosteric voltage-gating scheme greatly increases the minimal complexity of any model of Ca^{2+}-dependent activation. Previous work has demonstrated that mSlo exhibits a dose–response relationship for Ca^{2+} that is characterized by a Hill coefficient of ~1–3 (Cui et al., 1997). Thus, the channel must have at least three Ca^{2+} binding sites and it is reasonable to assume that there might four, one for each subunit. Given a 10-state model of voltage gating and four Ca^{2+} binding sites, a complete model of mSlo gating must contain a minimum of 50 states (for each state in the voltage-gating scheme there will exist at least one state with 0–4 Ca^{2+} ions bound). If Ca^{2+} binding affects voltage-sensor movement, a 70-state model is necessary. Even more states may be required if the relative position of Ca^{2+}-bound subunits and activated voltage sensors within the channel homotetramer affect their interaction (Cox et al., 1997a; Horrigan, F.T., and R.W. Aldrich, manuscript in preparation).

Limitations of the Data

According to Scheme IX, measurements of $\tau(I_K)$ and P_o at negative voltages provide direct information about the kinetics and voltage dependence of the C_0–O_0 transition. However, not all parameters in the allosteric

model are as tightly constrained, and several simplifying assumptions have been made that require confirmation. For example, the properties of closed-state transitions (C–C) were determined based upon analysis of the delay in I_K activation as well as the voltage dependence of $\tau(I_K)$ and P_o. These data are consistent with the assumption that horizontal transitions represent the activation of four independent and identical voltage sensors and that the forward and backward rate constants for these transitions are symmetrically voltage dependent. Similarly, the assumption that forward and backward rate constants for voltage-sensor activation are symmetrically affected by channel opening appears consistent with the presence of a brief delay in the decay of potassium tail currents. However, ionic current data provides only an indirect measurement of voltage-sensor movement, and deviations from these simple assumptions are possible.

It thus becomes important to characterize the properties of voltage-sensor movement. In the companion article (Horrigan and Aldrich, 1999), gating current measurements were used to directly examine voltage-sensor movement. The results generally confirm the above assumptions and provide further support for the allosteric voltage-gating scheme.

appendix

To derive an expression for the delay duration (Δt), Eq. 4 is rewritten in terms of open-state occupancy:

$$O(t) = O_\infty[1 - e^{(\Delta t - t)/\tau}] \qquad t \geq T, \tag{22}$$

where T is the time where $O(t)$ achieves an exponential time course, and τ is the time constant of I_K relaxation [$\tau(I_K)$]. dO/dt can then be defined after the delay:

$$O'(t) = \frac{O_\infty}{\tau} e^{(\Delta t - t)/\tau} \qquad t \geq T. \tag{23}$$

Combining Eqs. 22 and 23 gives:

$$\left[\frac{\tau O'(t)}{O(t) + \tau O'(t)}\right] = e^{(\Delta t - t)/\tau}. \tag{24}$$

Eq. 24 can be linearized when $[(\Delta t - t)/\tau]$ is small (when $O << \tau O'$). Such is the case for mSlo at $t = T$, when I_K achieves an exponential time course:

$$\left[\frac{\tau O'(T)}{O(T) + \tau O'(T)}\right] = 1 + \frac{(\Delta t - T)}{\tau}; \tag{25}$$

hence

$$\Delta t = T - \frac{O(T)}{O'(T)}. \tag{26}$$

Because $O(T)$ is small during the delay $O'(t)$ can be approximated by Eq. 10:

$$O'(t) = \delta C_L(t) \qquad t \leq T, \tag{27}$$

and

$$O(T) = \int_0^T O'(t)dt = \delta \int_0^T C_L(t)dt. \tag{28}$$

Combining Eqs. 26–28 gives:

$$\Delta t = T - \int_0^T \frac{C_L(t)dt}{C_L(T)}. \tag{29}$$

Thus Δt is determined only by $C_L(t)$. If transitions among closed states are assumed to be fast relative to channel opening, as in Scheme V, then the amplitude and time course of C_L should be functions mainly of voltage-dependent rate constants that characterize closed-state transitions.

In Scheme V, C_L can be expressed as the product of a voltage-dependent amplitude function ($F[v] = A_\infty^4$) and a time-dependent function of the voltage-sensor activation time constant τ_J $\{G(\tau_J[v],t) = [1 - e^{(-t/\tau_J)}]^4\}$ (see Eqs. 2 and 8):

$$C_L[v,t] = F[v]G(\tau_J[v],t). \tag{30}$$

For any model where C_L can be expressed in terms of Eq. 30, Eq. 29 can be expressed in terms of only $G[\tau_J[v], t]$:

$$\Delta t(\tau_J[v]) = T - \int_0^T \frac{G(\tau_J[v],t)dt}{G(\tau_J[v],T)}. \tag{31}$$

Thus Δt is a function of $\tau_J[v]$. Now we determine the conditions under which Δt will be proportional to $\tau_J[v]$ or, equivalently,

$$\frac{\Delta t(\tau_J[v_2])}{\Delta t(\tau_J[v_1])} = \frac{\tau_J[v_2]}{\tau_J[v_1]} = s \tag{32}$$

or

$$\Delta t[s\tau] = s\Delta t[\tau], \tag{33}$$

where $\tau = \tau_J[v_1]$ and $s\tau = \tau_J[v_2]$. If Eq. 33 is true, then, by combining Eqs. 31 and 33,

$$T - \int_0^T \frac{G[s\tau,t]dt}{G[s\tau,T]} = \left(T - \int_0^T \frac{G[\tau,t]dt}{G[\tau,T]}\right), \tag{34}$$

where

$$G[s\tau,t] = G_\infty \tag{35}$$

for $t \geq T$. Eq. 34 is true if

$$G[\tau,t] = G[s\tau,st] \tag{36}$$

(a condition that holds for Scheme V). Eq. 36 implies:

$$\int_0^T \frac{G[\tau,t]dt}{G[\tau,T]} = \int_0^T \frac{G[s\tau,st]dt}{G[s\tau,sT]}. \tag{37}$$

By changing the variable of integration ($r = st$) this becomes:

$$\int_0^T \frac{G[s\tau,st]dt}{G[s\tau,sT]} = \frac{1}{s}\int_0^T \frac{G[s\tau,r]dr}{G[s\tau,T]} = \frac{1}{s}\left(\int_0^T \frac{G[s\tau,r]dr}{G[s\tau,T]} + \int_T^{sT} \frac{G[s\tau,r]dr}{G[s\tau,T]}\right). \tag{38}$$

Given Eq. 35 then:

$$\frac{G[s\tau,r]dr}{G[s\tau,T]} = 1 \tag{39}$$

for $r \geq T$. Combining Eqs. 37–39 and replacing r with t yields:

$$\int_0^T \frac{G[\tau,t]dt}{G[\tau,T]} = \frac{1}{s}\left\{\int_0^{sT} \frac{G[s\tau,t]dt}{G[s\tau,T]} + T\,(s-1)\right\}, \tag{40}$$

which can be rearranged to yield Eq. 34. Thus Δt is proportional to $\tau_J[v]$ for Scheme V under the conditions that, first, I_K achieves an exponential time course when P_o is small and, second, transitions among closed states are assumed to be fast relative to channel opening.

We thank Dan Cox and Gargi Talukder for helpful comments on the manuscript.

This work was supported by a grant from the National Institutes of Health (NS23294) and by a National Institute of Mental Health Silvio Conte Center for Neuroscience Research grant (MH48108). R.W. Aldrich is an investigator with the Howard Hughes Medical Institute.

Submitted: 16 March 1999 Revised: 1 June 1999 Accepted: 7 June 1999

references

Aggarwal, S.K., and R. MacKinnon. 1996. Contribution of the S4 segment to gating charge in the *Shaker* K^+ channel. *Neuron* 16: 1169–1177.

Almers, W. 1978. Gating currents and charge movements in excitable membranes. *Rev. Physiol. Biochem. Pharmacol.* 82:96–190.

Armstrong, C.M., and F. Bezanilla. 1974. Charge movement associated with the opening and closing of the activation gates of the Na channels. *J. Gen. Physiol.* 63:533–552.

Bao, H., A. Hakeem, M. Henteleff, J.G. Starkus, and M.D. Rayner. 1999. Voltage-insensitive gating after charge-neutralizing mutations in the S4 segment of shaker channels. *J. Gen. Physiol.* 113:139–151.

Barrett, J.N., K.L. Magleby, and B.S. Pallotta. 1982. Properties of single calcium-activated potassium channels in cultured rat muscle. *J. Physiol.* 331:211–230.

Bielefeldt, K., and M.B. Jackson. 1993. A calcium-activated potassium channel causes frequency-dependent action-potential failures in a mammalian nerve terminal. *J. Neurophysiol.* 70:284–298.

Brayden, J.E., and M.T. Nelson. 1992. Regulation of arterial tone by activation of calcium-dependent potassium channels. *Science.* 256:532–535.

Cole, K.S., and J.W. Moore. 1960. Potassium ion current in the squid giant axon: dynamic characteristic. *Biophys. J.* 1:1–14.

Colquhoun, D., and A.G. Hawkes. 1977. Relaxation and fluctuations of membrane currents that flow through drug-operated channels. *Proc. R. Soc. Lond. B Biol. Sci.* 199:231–262.

Cox, D.H., J. Cui, and R.W. Aldrich. 1997a. Allosteric gating of a large conductance Ca-activated K^+ channel. *J. Gen. Physiol.* 110: 257–281.

Cox, D.H., J. Cui, and R.W. Aldrich. 1997b. Separation of gating properties from permeation and block in mslo large conductance Ca-activated K^+ channels. *J. Gen. Physiol.* 109:633–646.

Crest, M., and M. Gola. 1993. Large conductance $Ca^{(2+)}$-activated K^+ channels are involved in both spike shaping and firing regulation in helix neurones. *J. Physiol.* 465:265–287.

Cui, J., D.H. Cox, and R.W. Aldrich. 1997. Intrinsic voltage dependence and Ca^{2+} regulation of mslo large conductance Ca-activated K^+ channels. *J. Gen. Physiol.* 109:647–673.

Diaz, F., M. Wallner, E. Stefani, L. Toro, and R. Latorre. 1996. Interaction of internal Ba^{2+} with a cloned Ca^{2+}-dependent K^+ (hslo) channel from smooth muscle. *J. Gen. Physiol.* 107:399–407.

Diaz, L., P. Meera, J. Amigo, E. Stefani, O. Alvarez, L. Toro, and R. Latorre. 1998. Role of the S4 segment in a voltage-dependent calcium-sensitive potassium (hSlo) channel. *J. Biol. Chem.* 273: 32430–32436.

DiChiara, T.J., and P.H. Reinhart. 1995. Distinct effects of Ca^{2+} and voltage on the activation and deactivation of cloned Ca^{2+}-activated K^+ channels. *J. Physiol.* 489:403–418.

DiChiara, T.J., and P.H. Reinhart. 1997. Redox modulation of hslo Ca^{2+}-activated K^+ channels. *J. Neurosci.* 17:4942–4955.

Gorman, A.L., and M.V. Thomas. 1980. Potassium conductance and internal calcium accumulation in a molluscan neurone. *J. Physiol.* 308:287–313.

Hamill, O.P., A. Marty, E. Neher, B. Sakmann, and F.J. Sigworth. 1981. Improved patch-clamp techniques for high-resolution current recording from cells and cell-free membrane patches. *Pflügers Arch.* 391:85–100.

Herrington, J., and R.J. Bookman. 1995. Pulse Control. University of Miami Press, Miami, FL.

Hirschberg, B., A. Rovner, M. Lieberman, and J. Patlak. 1995. Transfer of twelve charges is needed to open skeletal muscle Na^+ channels. *J. Gen. Physiol.* 106:1053–1068.

Hodgkin, A.L., and A.F. Huxley. 1952. A quantitative description of membrane current and its application to conduction and excitation in muscle. *J. Physiol.* 117:500–544.

Holmgren, M., K.S. Shin, and G. Yellen. 1998. The activation gate of a voltage-gated K^+ channel can be trapped in the open state by an intersubunit metal bridge. *Neuron.* 21:617–621.

Horrigan, F.T., and R.W. Aldrich. 1999. Allosteric voltage-gating of potassium channels II: mSlo channel gating charge movement in the absence of Ca^{2+}. *J. Gen. Physiol.* 114:305–336.

Hudspeth, A.J., and R.S. Lewis. 1988. Kinetic analysis of voltage- and ion-dependent conductances in saccular hair cells of the bull-frog, *Rana catesbeiana*. *J. Physiol.* 400:237–274.

Islas, L.D., and F.J. Sigworth. 1996. The limiting slope of KV 2.1 channels shows a gating charge of about 12 e. *Biophys. J.* 70:A190. (Abstr.)

Lancaster, B., R.A. Nicoll, and D.J. Perkel. 1991. Calcium activates two types of potassium channels in rat hippocampal neurons in culture. *J. Neurosci.* 11:23–30.

Larsson, H.P., O.S. Baker, D.S. Dhillon, and E.Y. Isacoff. 1996. Transmembrane movement of the *Shaker* K^+ channel S4. *Neuron.* 16:387–397.

Latorre, R., C. Vergara, and C. Hidalgo. 1982. Reconstitution in planar lipid bilayers of a Ca^{2+}-dependent K^+ channel from transverse tubule membranes isolated from rabbit skeletal muscle. *Proc. Natl. Acad. Sci. USA.* 79:805–809.

Ledwell, J.L., and R.W. Aldrich. 1999. Mutations in the S4 region isolate the final voltage-dependent cooperative step in potassium channel activation. *J. Gen. Physiol.* 113:389–414.

Lewis, R.S., and A.J. Hudspeth. 1983. Voltage- and ion-dependent conductances in solitary vertebrate hair cells. *Nature.* 304:538–541.

Liu, Y., M. Holmgren, M.E. Jurman, and G. Yellen. 1997. Gated access to the pore of a voltage-dependent K^+ channel. *Neuron.* 19: 175–184.

Magleby, K.L., and B.S. Pallotta. 1983a. Burst kinetics of single calcium-activated potassium channels in cultured rat muscle. *J. Physiol.* 344:605–623.

Magleby, K.L., and B.S. Pallotta. 1983b. Calcium dependence of open and shut interval distributions from calcium-activated potassium channels in cultured rat muscle. *J. Physiol.* 344:585–604.

Mannuzzu, L.M., M.M. Moronne, and E.Y. Isacoff. 1996. Direct physical measure of conformational rearrangement underlying potassium channel gating. *Science.* 271:213–216.

Marks, T.N., and S.W. Jones. 1992. Calcium currents in the A7r5 smooth muscle–derived cell line. An allosteric model for calcium channel activation and dihydropyridine agonist action. *J. Gen. Physiol.* 99:367–390.

Marrion, N.V., and S.J. Tavalin. 1998. Selective activation of Ca^{2+}-activated K^+ channels by co-localized Ca^{2+} channels in hippocampal neurons. *Nature.* 395:900–905.

Marty, A. 1981. Ca-dependent K channels with large unitary conductance in chromaffin cell membranes. *Nature.* 291:497–500.

McCormack, K., W.J. Joiner, and S.H. Heinemann. 1994. A characterization of the activating structural rearrangements in voltage-dependent *Shaker* K^+ channels. [Published erratum appears in *Neuron*. 1994. 12:706.] *Neuron.* 12:301–315.

McManus, O.B., and K.L. Magleby. 1991. Accounting for the $Ca^{(2+)}$-dependent kinetics of single large-conductance $Ca^{(2+)}$-activated K^+ channels in rat skeletal muscle. *J. Physiol.* 443:739–777.

Meera, P., M. Wallner, Z. Jiang, and L. Toro. 1996. A calcium switch for the functional coupling between alpha (hslo) and beta subunits (KV,Ca beta) of maxi K channels. *FEBS Lett.* 382:84–88.

Methfessel, C., and G. Boheim. 1982. The gating of single calcium-dependent potassium channels is described by an activation/blockade mechanism. *Biophys. Struct. Mech.* 9:35–60.

Moczydlowski, E., and R. Latorre. 1983. Gating kinetics of Ca^{2+}-activated K^+ channels from rat muscle incorporated into planar lipid bilayers. Evidence for two voltage-dependent Ca^{2+} binding reactions. *J. Gen. Physiol.* 82:511–542.

Monod, J., J. Wyman, and J.P. Changeux. 1965. On the nature of allosteric transitions: a plausible model. *J. Mol. Biol.* 12:88–118.

Nelson, M.T., H. Cheng, M. Rubart, L.F. Santana, A.D. Bonev, H.J. Knot, and W.J. Lederer. 1995. Relaxation of arterial smooth muscle by calcium sparks. *Science.* 270:633–637.

Neyton, J. 1996. A Ba^{2+} chelator suppresses long shut events in fully activated high-conductance Ca^{2+}-dependent K^+ channels. *Biophys. J.* 71:220–226.

Noceti, F., P. Baldelli, X. Wei, N. Qin, L. Toro, L. Birnbaumer, and E. Stefani. 1996. Effective gating charges per channel in voltage-dependent K^+ and Ca^{2+} channels. *J. Gen. Physiol.* 108:143–155.

Pallotta, B.S., K.L. Magleby, and J.N. Barrett. 1981. Single channel recordings of Ca^{2+}-activated K^+ currents in rat muscle cell culture. *Nature.* 293:471–474.

Perozo, E., D.M. Cortes, and L.G. Cuello. 1998. Three-dimensional architecture and gating mechanism of a K^+ channel studied by EPR spectroscopy. *Nat. Struct. Biol.* 5:459–469.

Perozo, E., D.M. Papazian, E. Stefani, and F. Bezanilla. 1992. Gating currents in *Shaker* K^+ channels. Implications for activation and inactivation models. *Biophys. J.* 62:160–168. Discussion: 169–171.

Perutz, M. 1989. Mechanisms of cooperativity and allosteric regulation in proteins. Cambridge University Press, New York. pp. 101.

Petersen, O.H., and Y. Maruyama. 1984. Calcium-activated potassium channels and their role in secretion. *Nature.* 307:693–696.

Press, W.H., S.A. Teukolsky, W.T. Vetterling, and B.P. Flannery. 1992. Numerical recipes in C: the art of scientific computing, 2. Cambridge University Press, NY. 717–722.

Ríos, E., M. Karhanek, J. Ma, and A. Gonzalez. 1993. An allosteric model of the molecular interactions of excitation–contraction coupling in skeletal muscle. *J. Gen. Physiol.* 102:449–481.

Robitaille, R., M.L. Garcia, G.J. Kaczorowski, and M.P. Charlton. 1993. Functional colocalization of calcium and calcium-gated potassium channels in control of transmitter release. *Neuron.* 11: 645–655.

Rothberg, B.S., and K.L. Magleby. 1998. Kinetic structure of large-conductance Ca^{2+}-activated K^+ channels suggests that the gating includes transitions through intermediate or secondary states. A mechanism for flickers. *J. Gen. Physiol.* 111:751–780.

Safronov, B.V., and W. Vogel. 1998. Large conductance $Ca^{(2+)}$-activated K^+ channels in the soma of rat motoneurones. *J. Membr. Biol.* 162:9–15.

Schoppa, N.E., K. McCormack, M.A. Tanouye, and F.J. Sigworth. 1992. The size of gating charge in wild-type and mutant *Shaker* potassium channels. *Science.* 255:1712–1715.

Schoppa, N.E., and F.J. Sigworth. 1998a. Activation of *Shaker* potassium channels. I. Characterization of voltage-dependent transitions. *J. Gen. Physiol.* 111:271–294.

Schoppa, N.E., and F.J. Sigworth. 1998b. Activation of *Shaker* potassium channels. III. An activation gating model for wild-type and V2 mutant channels. *J. Gen. Physiol.* 111:313–342.

Schreiber, M., and L. Salkoff. 1997. A novel calcium-sensing domain in the BK channel. *Biophys. J.* 73:1355–1363.

Schreiber, M., A. Yuan, and L. Salkoff. 1999. Transplantable sites confer calcium sensitivity to BK channels. *Nat. Neurosci.* 2:416–421.

Seoh, S.A., D. Sigg, D.M. Papazian, and F. Bezanilla. 1996. Voltage-sensing residues in the S2 and S4 segments of the *Shaker* K^+ channel. *Neuron.* 16:1159–1167.

Shen, K.Z., A. Lagrutta, N.W. Davies, N.B. Standen, J.P. Adelman, and R.A. North. 1994. Tetraethylammonium block of Slowpoke calcium-activated potassium channels expressed in *Xenopus* oocytes: evidence for tetrameric channel formation. *Pflügers Arch.* 426:440–445.

Sigg, D., and F. Bezanilla. 1997. Total charge movement per channel. The relation between gating charge displacement and the voltage sensitivity of activation. *J. Gen. Physiol.* 109:27–39.

Sigworth, F.J. 1994. Voltage gating of ion channels. *Q. Rev. Biophys.* 27:1–40.

Sigworth, F.J., and J. Zhou. 1992. Ion channels. Analysis of nonstationary single-channel currents. *Methods Enzymol.* 207:746–762.

Smith-Maxwell, C.J., J.L. Ledwell, and R.W. Aldrich. 1998. Uncharged S4 residues and cooperativity in voltage-dependent potassium channel activation. *J. Gen. Physiol.* 111:421–439.

Stefani, E., M. Ottolia, F. Noceti, R. Olcese, M. Wallner, R. Latorre, and L. Toro. 1997. Voltage-controlled gating in a large conductance Ca^{2+}-sensitive K^+channel (hslo). *Proc. Natl. Acad. Sci. USA.* 94:5427–5431.

Storm, J.F. 1987. Action potential repolarization and a fast afterhyperpolarization in rat hippocampal pyramidal cells. *J. Physiol.* 385:733–759.

Tytgat, J., and P. Hess. 1992. Evidence for cooperative interactions in potassium channel gating. *Nature.* 359:420–423.

Unwin, N. 1998. The nicotinic acetylcholine receptor of the Torpedo electric ray. *J. Struct. Biol.* 121:181–190.

Unwin, N., C. Toyoshima, and E. Kubalek. 1988. Arrangement of the acetylcholine receptor subunits in the resting and desensitized states, determined by cryoelectron microscopy of crystallized *Torpedo* postsynaptic membranes. *J. Cell Biol.* 107:1123–1138.

Unwin, P.N., and P.D. Ennis. 1984. Two configurations of a channel-forming membrane protein. *Nature.* 307:609–613.

Vandenberg, C.A., and F. Bezanilla. 1991. A sodium channel gating model based on single channel, macroscopic ionic, and gating currents in the squid giant axon. *Biophys. J.* 60:1511–1533.

Wei, A., C. Solaro, C. Lingle, and L. Salkoff. 1994. Calcium sensitivity of BK-type K_{Ca} channels determined by a separable domain. *Neuron.* 13:671–681.

Wyman, J., and S.J. Gill. 1990. Binding and Linkage: functional chemistry of biological macromolecules. University Science Books, Mill Valley, CA. pp. 330.

Yang, N., A.J. George, and R. Horn. 1996. Molecular basis of charge movement in voltage-gated sodium channels. *Neuron.* 16:113–122.

Yang, N., and R. Horn. 1995. Evidence for voltage-dependent S4 movement in sodium channels. *Neuron.* 15:213–218.

Yazejian, B., D.A. DiGregorio, J.L. Vergara, R.E. Poage, S.D. Meriney, and A.D. Grinnell. 1997. Direct measurements of presynaptic calcium and calcium-activated potassium currents regulating neurotransmitter release at cultured *Xenopus* nerve-muscle synapses. *J. Neurosci.* 17:2990–3001.

Yusaf, S.P., D. Wray, and A. Sivaprasadarao. 1996. Measurement of the movement of the S4 segment during the activation of a voltage-gated potassium channel. *Pflügers Arch.* 433:91–97.

Zagotta, W.N., T. Hoshi, and R.W. Aldrich. 1994a. *Shaker* potassium channel gating. III: Evaluation of kinetic models for activation. *J. Gen. Physiol.* 103:321–362.

Zagotta, W.N., T. Hoshi, J. Dittman, and R.W. Aldrich. 1994b. *Shaker* potassium channel gating. II: Transitions in the activation pathway. *J. Gen. Physiol.* 103:279–319.